# Comparing satellite and ground–based observations of cloud occurrence over high southern latitudes

**Cameron McErlich[1], Adrian McDonald[1,2], Alex Schuddeboom[1], and Israel Silber[3]**

[1]School of Physical and Chemical Sciences, University of Canterbury, Christchurch, New Zealand
[2]Gateway Antarctica, University of Canterbury, Christchurch, New Zealand
[3]Department of Meteorology and Atmospheric Science, Pennsylvania State University, University Park, PA, USA

**Key Points:**

- 2BCL5 and DARDAR cloud occurrences show large differences at low-levels globally, with the largest disparities at high southern latitudes
- Comparison with Antarctic ground observations tentatively suggests that this difference is likely due to false detections in DARDAR
- 2BCL5 and DARDAR cloud phase estimates do not adhere to physical constraints set by temperature from ECMWF-AUX or local radiosondes

Corresponding author: Cameron McErlich, cameron.mcerlich@pg.canterbury.ac.nz

**Abstract**

The 2B-CLDCLASS-LIDAR R05 (2BCL5) and the raDAR/liDAR (DARDAR) satellite retrievals of cloud occurrence are compared as a function of altitude and latitude. The largest disparities are observed at low altitudes over high southern latitudes. These datasets are cross referenced to ground–based measurements from the Atmospheric Radiation Measurement (ARM) West Antarctic Radiation Experiment (AWARE) campaign at McMurdo Station, Antarctica. Compared to AWARE observations, both 2BCL5 and DARDAR underestimate cloud occurrence below 1.5 km, with 2BCL5 and DARDAR distinguishing roughly one third of cloud occurrences observed by AWARE at 0.5 km. While DARDAR identifies greater cloud occurrences than 2BCL5 below 1.5 km, cloud occurrence values for the two datasets have similar differences relative to ground-based measurements. Therefore, the DARDAR retrievals of greater cloud occurrence at low altitudes are likely due to a larger quantity of false positives associated with radar ground clutter or attenuated lidar retrievals. DARDAR cloud occurrences match better with AWARE than 2BCL5 above 5 km. However, the likely underestimation of ground-based measurements at higher altitudes suggests DARDAR may underestimate high level cloud occurrence. Finally, both datasets indicate the presence of liquid containing clouds at temperatures within the homogeneous freezing regime, despite the fact that the ECMWF-AUX dataset implemented in their processing clearly indicates temperatures below -38 °C. Using AWARE radiosonde (ECMWF-AUX) temperature data, we find that 2BCL5 detects 13.3% (13.8%) of mixed phase clouds below -38 °C, while DARDAR detects 5.7% (6.6%) of mixed phase and 1.1% (1.3%) of liquid phase clouds below -38 °C.

## 1 Introduction

Clouds play a critical role in the Earth's energy balance. They can act to cool the surface by reflecting incoming solar radiation back into space or warm the surface by absorbing outgoing infrared radiation and re-radiating it toward the surface (Marshall & Plumb, 2008). Although all clouds have an effect on the climate, clouds over the oceans are especially important due to the strong contrast in albedo between the sea surface and clouds. This means that the surface radiation budget over the ocean is more sensitive to cloud coverage than over land (Cess, 1990). These effects are greatest over the Southern Ocean which has an annual mean cloud coverage of around 80% – 90% (e.g., Kay et al., 2012; McCoy et al., 2014; Matus & L'ecuyer, 2017).

In this study, satellite measurements are used to evaluate cloud occurrence and cloud phase over Southern Hemisphere high latitudes. Due to the limitations of satellite–based datasets in this region, a ground–based dataset is needed for independent examination of low level cloud. Unfortunately, ground–based measurements which vertically resolve cloud and cloud phase over the Southern Ocean are very rare due to the complicated logistics associated with collecting measurements from shipborne platforms. As such, ground–based measurements from the AWARE campaign over McMurdo Station in Antarctica are used as a representation of cloud at southern high latitudes. The AWARE dataset provides detailed cloud occurrence and phase measurements described in more detail in section 2.4, and is used for comparison with satellite–based measurements.

Comparisons between observations and models indicate significant shortwave radiation biases over the Southern Ocean with magnitudes of up to 30 $Wm^{-2}$ (Trenberth & Fasullo, 2010). This shortwave bias induces warm sea surface temperature biases in climate simulations (Hyder et al., 2018), which limit the accuracy of models. The shortwave bias observed in the Southern Ocean has been identified as a contributory factor in a number of issues in models, such as the double–Intertropical Convergence Zone (e.g., Hwang & Frierson, 2013), errors in the meridional energy transport (e.g., Mason et al., 2015), biases in the position of the Southern Hemisphere storm track (e.g., Ceppi et al., 2012) and the intensity of the Southern Hemisphere jet (e.g., Kay et al., 2016). Reduc-

tion of the shortwave bias over the Southern Ocean is thus critical to improving the simulation of climate at the Southern hemisphere mid- to high-latitudes.

Identifying the sources of these biases in climate models is an active and ongoing area of research. Though, Hyder et al. (2018) identified that 70% of the sea surface temperature bias in the Coupled Model Intercomparison Project Phase 5 (CMIP5) climate models relative to observations can be attributed to issues associated with the representation of clouds. Other work has shown that problems with the models include simulating too little cloud cover (e.g., Bodas-Salcedo et al., 2012; Schuddeboom et al., 2018; Kuma et al., 2020), excessive sunlight absorbed by the ocean surface (e.g., Trenberth & Fasullo, 2010; Hyder et al., 2018), a lack of clouds in the cold sectors of cyclones (e.g., Bodas-Salcedo et al., 2014), and a lack of reflective supercooled water clouds (e.g., Bodas-Salcedo et al., 2016; Kuma et al., 2020). Work has also shown that the bias over the Southern Ocean is not a single issue since there are different biases at higher and lower latitudes (Schuddeboom et al., 2019; Kuma et al., 2020).

Ice hydrometeors and water droplets have differing radiative properties and therefore reflect and absorb different levels of incoming shortwave radiation (e.g., Haynes et al., 2011; Scott & Lubin, 2014; Vergara-Temprado et al., 2018). Previous work has identified that supercooled clouds are very common over the Southern Ocean (e.g., Chubb et al., 2013; Jolly et al., 2018; Listowski et al., 2018; Morrison et al., 2011) and are potentially a major contributor to known model biases (e.g., Bodas-Salcedo et al., 2016; Kay et al., 2016; Kuma et al., 2020). In particular, Bodas-Salcedo et al. (2016) identified that clouds with supercooled tops contribute between 27 and 38% to the total reflected solar radiation over the Southern Ocean, and suggested that climate models poorly simulate these clouds. Models that overestimate the amount of ice cloud will produce a positive shortwave radiation bias, due to changes in the cloud albedo. As the introduction of ice into supercooled liquid clouds also causes the rapid growth of ice crystal at the expense of the liquid droplets (Vergara-Temprado et al., 2018), a minor error representing cloud phase can have large impacts.

Boundary layer observations by satellite instruments are limited by the presence of an almost continuous cloud cover in the Southern Ocean which acts to obscure low-level clouds. Unfortunately, measurements from satellites using passive instruments such as the Moderate Resolution Imaging Spectroradiometer (MODIS; Salomonson et al., 2002) and the International Satellite Cloud Climatology Project (ISCCP; Rossow & Schiffer, 1999) can only observe radiation scattered or emitted from the cloud top of optically thick clouds. Therefore, one can accurately identify the cloud properties at the top of the cloud with passive instruments, but cannot resolve the full vertical profile of clouds in most cases. Instead, active instruments such as those aboard the CloudSat and Cloud–Aerosol Lidar and Infrared Pathfinder Satellite Observation (CALIPSO) satellites need to be used to investigate cloud vertical structure.

Due to the limitations of satellite observations in the lower troposphere, ground based measurements from sub–Antarctic and Antarctic sites can provide essential information about cloud vertical structure. Surface based lidar instruments can detect layers of liquid water in the boundary layer, but similar to space–borne lidars, their signal becomes attenuated by optically thick cloud. Ground based radars can penetrate through these optically thick clouds, but miss a portion of the optically and geometrically thin high-altitude ice clouds due to a lack of sensitivity (Protat et al., 2006, 2010).

## 2 Datasets and Methods

### 2.1 The CloudSat and CALIPSO satellites

The satellite datasets used in this study are merged products created from CloudSat and CALIPSO observations. Launched together in April 2006, these satellites fol-

low each other closely in orbit, initially as part of the A-Train constellation of satellites occupying a low Earth orbit (Stephens et al., 2002) and their measurements can be used to investigate the vertical distribution and properties of cloud. A partial equipment failure in 2017 forced CloudSat into a lower orbit to preserve the longevity of the instrument. CALIPSO was also moved into this lower orbit so that the two could continue to be used in conjunction. CloudSat has operated in daylight-only mode since 2011 due to a battery anomaly, which has inhibited nighttime measurements and reduced the quality of measurements collected during the sunlit portion of its orbit (Nayak, 2012).

The Cloud Profiling Radar (CPR), a 94 GHz radar that uses 3.3 $\mu$s pulses, is the primary instrument onboard the CloudSat satellite (Stephens et al., 2002). The main instrument onboard CALIPSO is the Cloud-Aerosol Lidar with Orthogonal Polarization (CALIOP) (Winker et al., 2007). CALIOP transmits two laser pulses at wavelengths of 1064 nm and 532 nm simultaneously and measures backscatter data at two polarisations. The backscattered signal is used to derive vertical profiles of aerosol and cloud properties, and the ratio of backscatter at the two wavelengths is used to discriminate between clouds and aerosols as well as to determine the composition of cloud (Winker et al., 2009; Z. Liu, 2009). The lidar depolarisation ratio can also be used to estimate the phase of scattering hydrometeors as either ice or liquid water (Sassen, 1991; Hu et al., 2009). CloudSat's CPR, has a horizontal footprint of 1.4 km x 1.8 km, and vertical resolution of 485 m up to a height of 25km (Stephens et al., 2008). CloudSat uses the strength of the signal reflected off hydrometeors to determine cloud vertical structure. However, CloudSat is affected by surface clutter below approximately 1.2 km (cf. Marchand et al., 2008; Tanelli et al., 2008) while the CALIPSO lidar signal is attenuated by passing through optically thick cloud.

### 2.2 The 2BCL5 data product

In this study we use the 2B-CLDCLASS-LIDAR R05 (2BCL5) dataset generated by combining measurements from CloudSat and CALIPSO to determine the vertical distribution of clouds, cloud phase, and cloud type (Sassen et al., 2008; Wang, 2019). Because of the different horizontal and vertical resolutions of the two instruments, data from several CALIOP footprints are matched to the larger CPR footprints. Unfortunately, the CALIOP linear depolarisation ratio measurement is limited by the attenuation of the lidar signal through thick clouds, so the 2BCL5 data product does not use this data to derive cloud phase. Instead, differences between the number concentration, vertical distribution and radiative properties of ice particles and water droplets are used to generate a temperature dependent radar reflectivity ($Z_e$) threshold (cf. Zhang et al., 2010). This $Z_e$ threshold is used alongside the integrated attenuated lidar backscattering coefficient and cloud base and top temperatures to distinguish between ice, liquid, and mixed phases cloudy air volumes (see Wang, 2019). The 2BCL5 product uses ancillary data from the ECMWF-AUX (Partain, 2007) product to provide temperature data.

Using 2BCL5 observations from 2016, cloud occurrence is derived as a function of altitude for different cloud phases. The vertical extent of the cloud is determined using the CloudLayerBase and CloudLayerTop fields. Cloud occurrence is assigned to each vertical bin between the cloud base and cloud top using the Cloud Fraction field. This process is repeated for each separate cloud layer in the 2BCL5 detection. Further partitioning using information about the three phase classification options, produces separate cloud masks for each phase. Profiles are summed and then normalised by using the total number of measurements.

### 2.3 The DARDAR data product

The second satellite dataset used in this study is the raDAR/liDAR (DARDAR) dataset. DARDAR is also a merged product derived from CloudSat and CALIPSO mea-

surements (Delanoë & Hogan, 2010), and uses ancillary temperature information from ECMWF-AUX. It therefore uses identical inputs to the 2BCL5 dataset. DARDAR v.2.11 (Ceccaldi et al., 2013) was also obtained for 2016, chosen to coincide with ground based measurements also used in this study. DARDAR provides vertically resolved profiles of cloud phase, identifying ice, mixed and liquid phase clouds. The phase determination algorithm also requires thermodynamic variables taken from the ECMWF-AUX product. Similarly to 2BCL5, CALIPSO footprints are matched to CloudSat resolution for merging. DARDAR has resolutions of 60 m in the vertical and 1 km in the horizontal. DARDAR cloud phase classification processes are detailed in Delanoë and Hogan (2010), but were updated in Ceccaldi et al. (2013) upon the release of the DARDAR v2 product.

DARDAR cloud measurements are grouped into a categorization mask that separates cloud into different categories. While it includes cloud features such as the location of supercooled water and ice hydrometeors, it also contains features such as aerosols and ground clutter not relevant to this study. To produce vertical profiles of cloud occurrence, the appropriate features (such as supercooled and water cloud) are selected to partition the data into clouds masks associated with the different phases. As for 2BCL5, these cloud masks are combined to generate cloud occurrences. Cloud occurrence profiles for each phase are merged by summing the cloud occurrence across each vertical level and normalised using the total number of measurements.

### 2.4 The AWARE dataset

The ground–based observations obtained during the 2016 Atmospheric Radiation Measurement (ARM) West Antarctic Radiation Experiment (AWARE) field campaign in Antarctica are used in this study. The AWARE campaign took place between November 2015 and January 2017 (Lubin et al., 2020), primarily at McMurdo Station (77.85°S, 166.72°E), and provides an unprecedented cloud and radiation dataset in this region (Lubin et al., 2020). In this study, we focus on AWARE measurements of cloud occurrence, cloud phase, and temperature.

The AWARE dataset used in this study includes hourly cloud masks generated from Ka-Band ARM Zenith Radar (KAZR; Widener et al., 2012) and the High Spectral Resolution Lidar (HSRL; Eloranta, 2005) measurements from McMurdo Station. These measurements are then gridded onto a fixed 7.5 m and 10 s vertically- and temporally-spaced grid, as detailed in Silber et al. (2018). This dataset spans from 1 January to 31 December 2016. KAZR was operated in two interleaved modes; a moderate sensitivity mode was used to detect upper–tropospheric clouds and a general mode used to detect lower–tropospheric clouds. We also use radiosonde soundings of temperature gathered twice daily and linearly gridded to the vertical grid of the hourly cloud masks (cf. Silber et al., 2018). AWARE observations include a significant quantity of cloud observations whose phase could not be identified, particularly at high altitudes, due to the attenuation of the lidar signal.

Both the KAZR and HSRL datasets have a high uptime, with more than 97% total data availability during 2016 (Silber et al., 2018). However, specific hours with low data availability might still cause a potential sampling bias in our analysis. Therefore, we set a hourly KAZR and HSRL data availability threshold of 75% (45 min) for cloud profiles to be considered in this analysis, this effectively rejects 2.3% of the AWARE dataset.

### 2.5 Combined Satellite and Ground-based Processing

To inter-compare the AWARE, 2BCL5 and DARDAR datasets, all of the observational datasets need to be constrained both spatially and temporally. First the satellite data was masked so that only observations falling within a 5 degree by 5 degree lat-

itude/longitude box centered on McMurdo Station were used. The AWARE data was also masked so that only measurements within 3 hours before or after a CloudSat/CALIPSO overpass are considered. All measurements from CloudSat/CALIPSO and the AWARE datasets include both cloud and precipitation masks. Only the months of January, October, November and December had significant quantities of coincident satellite and ground based observations. The passes used for comparison with the AWARE dataset were further filtered to only include passes where both 2BCL5 and DARDAR have concurrent observations, which gave a total of 180 passes.

The observational region was identified so that it would be large enough to contain a considerable number of satellite passes, but small enough to exclude the Trans-Antarctic mountains. The temporal coincidence was chosen to ensure that the different instruments would observe the same synoptic weather patterns. Work by Coggins et al. (2014) used the k–means clustering technique to produce a synoptic climatology of the Ross Sea and Ross Ice Shelf regions and identified the characteristic time periods of each synoptic state in the region persisted for between 13 and 20 hours. A later study by Jolly et al. (2018) used this synoptic climatology to quantify the vertical distribution of cloud occurrence, phase, and type over the Ross Ice Shelf and southern Ross Sea, which encompasses McMurdo Station. They found large differences between the synoptic regimes relative to seasonal variation for the cloud occurrence as a function of altitude (see also Silber et al., 2019). An additional study in which examined Eulerian cloud persistence using the AWARE data was also carried out by Silber et al. (2018). They investigated the persistence of all cloud layers, as well as those that necessarily contain liquid water, and reported a mean cloud persistence between 5 and 10 hours depending on the month. However, liquid-containing cloud layers have a much shorter mean persistence of 2.7 hours and 54% do not last for more than an hour. A temporal threshold of 1 hour from either side of the closest AWARE measurement during a satellite overpass (a 3 hour window in total) was selected based on these studies.

# 3 Results

## 3.1 Global distribution of satellite–based cloud occurrences

Before using the ground–based AWARE observations, the 2BCL5 and DARDAR datasets are directly compared. Figure 1 shows the latitudinal cloud occurrence as a function of altitude for the 2BCL5 dataset during 2016. While only 2016 is examined the mean values used in this analysis are representative of other years (analysis not shown). Figure 1 displays cloud occurrence for the ice, mixed and liquid cloud phases, as well as the combined total alongside temperature isotherms generated using monthly averages of ECMWF-AUX temperature profiles (Partain, 2007). The 0 °C isotherm identifies the location where liquid hydrometeors will begin to freeze into ice phase cloud; at higher temperatures only liquid phase cloud should generally be present. The -38 °C isotherm was chosen to represent the edge of the homogeneous freezing regime (Lamb & Verlinde, 2011). Below this temperature any supercooled water present in the cloud will freeze into ice crystals, such that only ice phase clouds will be present. Between the two thresholds there will be a combination of ice and supercooled water, so liquid, ice and mixed phase clouds can be present.

A notable feature of Figure 1 is a sharp reduction in the amount of cloud detected by 2BCL5 below an altitude of 1 km, present across all latitudes and phases. This highlights limitations in the 2BCL5 dataset at detecting cloud below this altitude. Figure 1b shows that ice phase cloud is absent in the tropical and subtropical regions below 5 km, where temperatures are higher, although there are some places below the 0 °C isotherm where ice phase clouds are present. Figure 1c shows that mixed phase clouds are generally present at altitudes above the -38 °C isotherm and below the 0 °C isotherm. Figure 1d shows liquid phase cloud at temperatures higher than 0 °C, which is plausible due

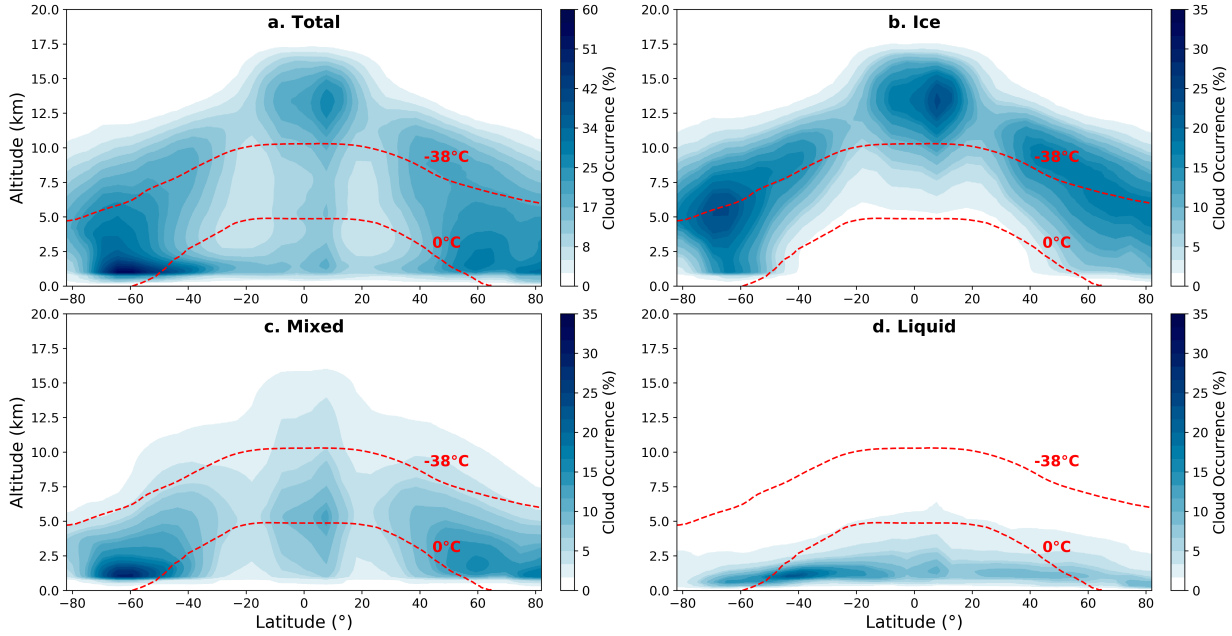


**Figure 1.** Latitudinal distribution of cloud occurrence as a function of altitude for the (a) total amount of cloud occurrence, as well as the (b) ice , (c) mixed and (d) liquid phases derived from the 2BCL5 observations from 2016. The dashed lines indicate isotherms of constant temperature generated using ECMWF-AUX temperature information.

to the presence of supercooled water below 0 °C. However, as the 2BCL5 liquid classification does not distinguish supercooled water further analysis assessing the quality of liquid phase partitioning cannot be done. The reduction of cloud observed by 2BCL5 below 1 km has particular implications over the Southern Ocean (50 °S - 75 °S) where low level cloud occurrence peaks, but where it is also considered to be underestimated in models (Bodas-Salcedo et al., 2012; Schuddeboom et al., 2018; Kuma et al., 2020).

Figure 2 shows the differences between DARDAR and 2BCL5 cloud occurrence rates as a function of latitude and altitude. As 2BCL5 and the DARDAR datasets are generated from the same satellite data, any differences between these two datasets is a result of the dataset processing. Figure 2a shows that overall 2BCL5 detects more cloud than DARDAR, except below 1 km where DARDAR identifies greater cloud occurrences. These differences are greatest near 65 °S, over the Southern Ocean and Antarctic region. When the total cloud occurrence is partitioned into the ice, mixed, and liquid cloud phases further differences between the datasets become apparent. Figure 2c shows that 2BCL5 always detects a larger occurrence of mixed phase cloud than the DARDAR dataset, with an absolute difference up to 25% over the Southern Ocean maximum at approximately 65S. DARDAR classifies these clouds as either ice or liquid depending on temperature, as can be seen in Figure 2b and Figure 2d. Figure 2b also shows a clear regional separation of the 2BCL5 and DARDAR data. The difference between these regions match well with the position of the -38 °C isotherm, with DARDAR detecting more ice phase cloud in between the 0 and -38 °C isotherms than the 2BCL5 dataset. Figure 2a shows only small differences in 2BCL5 and DARDAR cloud occurrence between these isotherms, indicating the differences must be a result of the phase identification algorithms. Figure 2d shows DARDAR detects more liquid phase clouds below the 0 °C isotherm, with 2BCL5 classifying the cloud in this region as mixed phase cloud (Figure 2c). Some portion of the observations classified as mixed phase cloud by the 2BCL5 algorithm also lie

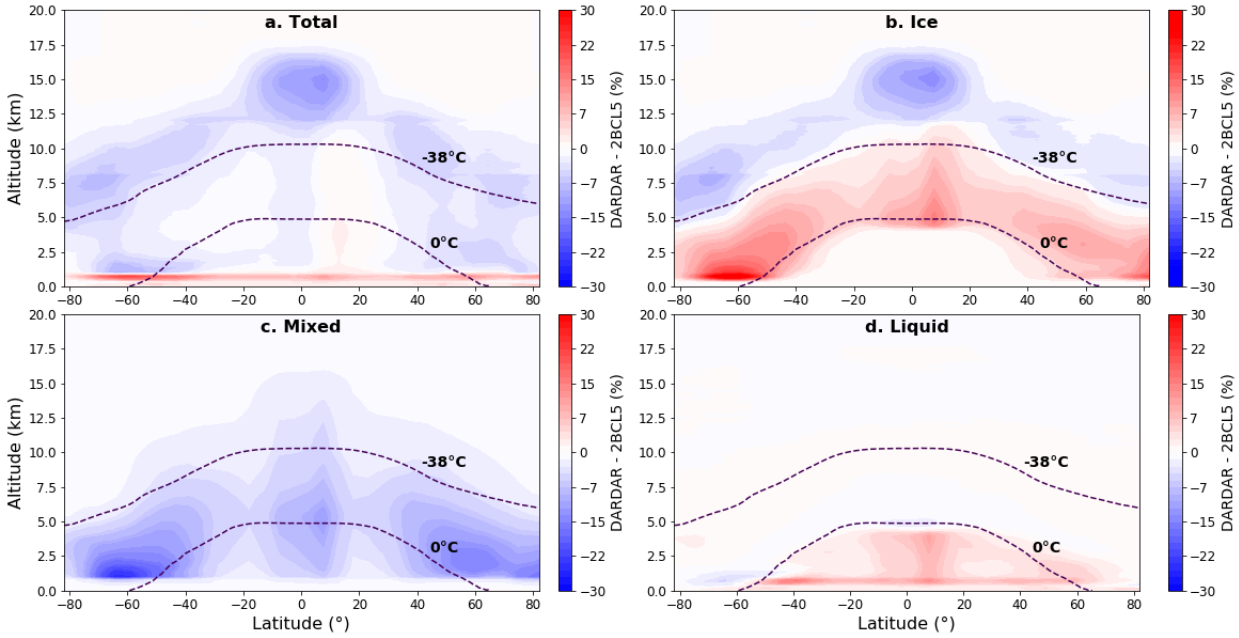


**Figure 2.** Differences in cloud occurrence between DARDAR and 2BCL5 during 2016, broken into (a) the total amount of cloud occurrence and (b) ice, (c) mixed and (d) liquid phase components. A positive value indicates DARDAR has a greater cloud occurrence than the 2BCL5 product. The dashed lines indicate isotherms of constant temperature generated using ECMWF-AUX temperature information.

outside the 0 °C and -38 °C isotherms, which disagrees with the physical limitations on cloud phase set by the temperature constraints defined by the ECMWF-AUX model output.

### 3.2 Cloud occurrence as a function of altitude

The greatest differences in cloud occurrence between 2BCL5 and DARDAR lie in their representation of low–level clouds over the Southern Ocean. This provides a strong motivation for a more detailed investigation of this region which includes the usage of ground based radar/lidar data. The cloud occurrence rate over McMurdo Station as a function of altitude for each of the AWARE, 2BCL5 and DARDAR datasets is shown in Figure 3. These profiles are shown individually for January, October, November and December. Cloud profiles for each satellite overpass are averaged over the month and split into their constituent phases. The filled curves in Figure 3 represent the DARDAR (a-d) and 2BCL5 (e-h) cloud occurrences and the dashed curves represent the AWARE observations.

The AWARE cloud profiles show limited amounts of liquid phase clouds. These clouds are confined to the bottom 4 km of the atmosphere except during December (Figure 3d) where liquid phase clouds occur up to an altitude of 4.5 km. Liquid phase clouds have a maximum occurrence rate of 5%, with no obvious vertical structure across the months examined. The AWARE ice cloud phase extends much higher than the liquid phase cloud, but shows reduced frequency above an altitude of 4 km. This reduction is balanced by an increase in cloud occurrence in the 'unknown' phase category. Ice phase cloud peaks at an altitude below 1 km during January and October (Figure 3a-b), but peaks at 2–2.5 km during November and December (Figure 3c-d). The unknown phase clouds in the

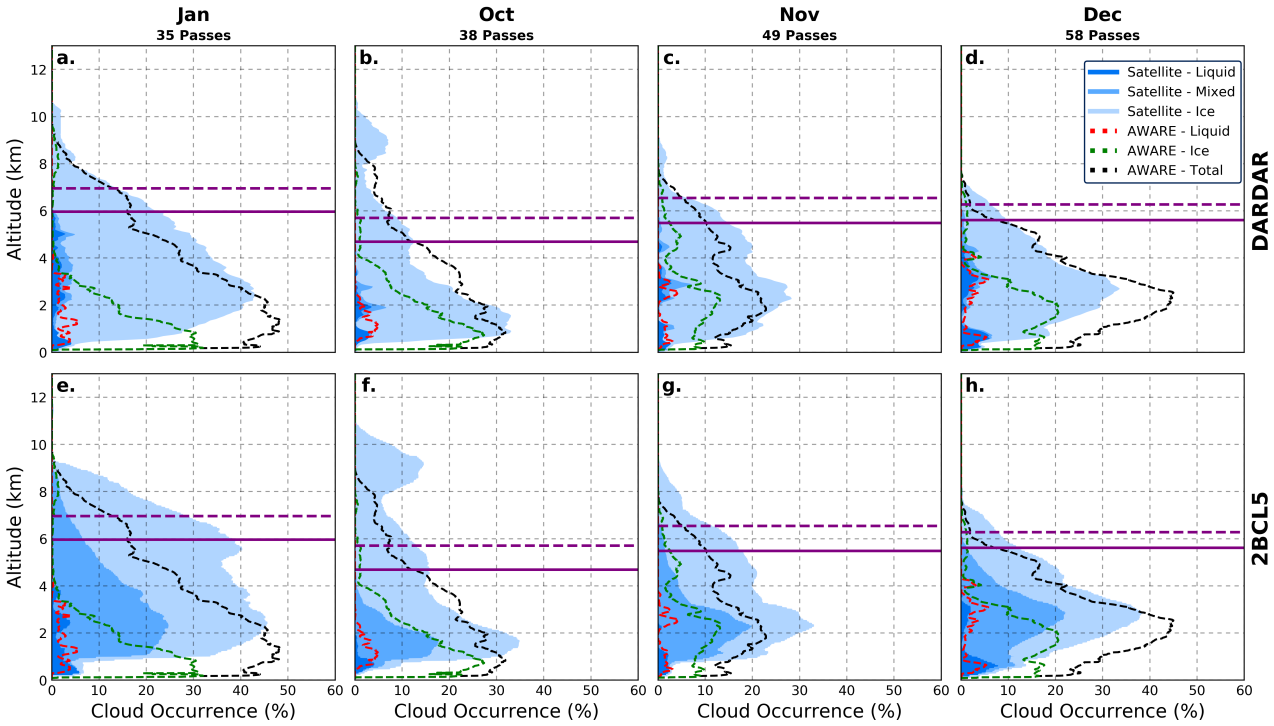


**Figure 3.** Mean vertical profiles of cloud occurrence for different cloud phases derived from observations over McMurdo Station during 2016. The dashed lines represent the AWARE cloud occurrence and the filled curves represent coincident DARDAR (a - d) and 2BCL5 (e - h) cloud occurrences. The number of passes are annotated at the top of the figure. The purple lines represents the mean (solid) and maximum (dashed) altitudes of the -38 °C isotherm across all passes, derived from twice-daily radiosonde observations.

AWARE dataset dominate the cloud occurrence above altitudes of 4 km in all months, due to the extinction of the lidar signal preventing classification of the cloud phase. The altitudes at which the clouds are most commonly classified as unknown phase are the same altitudes at which ice phase clouds dominate the satellite datasets. This highlights that the unknown phase class predominantly represents ice (volume-wise) as also noted by (cf. Silber et al., 2018). Previous work detailed in (Jolly et al., 2018) also supports this interpretation.

Figure 3a-d shows that the DARDAR cloud occurrence vertical profiles have liquid-containing clouds that extend up to an altitude of 6 km and a maximum occurrence of just over 5%. Mixed phase clouds are detected in the same altitude range as liquid phase clouds, but have a lower occurrence. The majority of DARDAR-detected clouds are classified as ice phase and extend to an altitude of 10 km. The cloud occurrence maxima for ice phase cloud generally occurs between 2 and 3 km, but is observed at a lower altitude during October (Figure 3b). Below this maxima, DARDAR cloud occurrence falls rapidly to values less than 10% below 1 km. No liquid or mixed phase cloud is identified in the DARDAR dataset above the monthly maximum level of the -38 °C isotherm, indicating DARDAR is conforming to liquid and mixed phase temperature constraints correctly.

Figure 3e-h identify vertical profiles of cloud occurrence for the 2BCL5 data product. These shows liquid phase cloud occurrences of up to 10% between the surface and 5 km, with the maximum occurrence between 0.3 and 1 km. Liquid phase cloud occur-

rence tends to drop off rapidly at altitudes above the maxima, although this drop is not as rapid in the summer months (December and January). The maximum occurrence of mixed phase cloud is consistent over all the examined months, falling between 2 and 3 km. October (Figure 3f) has the lowest quantity of mixed phase clouds compared to other months and shows no mixed phase cloud occurrence above 4 km. This is likely a reflection of the low altitude of the -38 °C isotherm in this month. Interestingly, the other months show mixed phase clouds up to 6.5km, meaning that clouds are observed above the maximum level of the -38 °C temperature isotherm derived from radiosondes. In particular, in January mixed phase clouds are present up 9 km which is much higher than the 7 km maximum of the -38 °C isotherm (Figure 3e). This shows clear limitations in how the 2BCL5 mixed phase cloud occurrence is determined with respect to temperature. The representation of cloud phase in the DARDAR dataset is better confined by the -38 °C isotherm than 2BCL5.

Comparison of the monthly mean cloud occurrence profiles from the two satellite datasets in the vicinity of McMurdo station shows that the 2BCL5 dataset has systematically higher cloud occurrences than the DARDAR dataset, except below 1 km where DARDAR has a higher occurrence of cloud than the 2BCL5 dataset. This matches with the global result displayed in Figure 2. Although these datasets differ, the relationship between cloud occurrence and altitude is similar in both datasets in general.

Comparison of the cloud occurrence profiles show that at a higher altitude the AWARE dataset likely underestimates cloud compared to the satellites datasets and at lower altitudes there is an underestimation of 2BCL5 and DARDAR cloud occurrences compared to AWARE. The satellite–based datasets are unable to detect a high number of clouds below 1 km, and conversely, the ground–based measurements are unable to detect as many clouds as 2BCL5 above 4km. As AWARE observations are often attenuated at higher altitudes, the good match with DARDAR observed might suggest that DARDAR is actually underestimating cloud occurrence. Therefore, we postulate that differences between 2BCL5 and DARDAR above 1 km are a result of an underestimation in DARDAR cloud occurrence. The discrepancy between the satellite– and ground–based peak in cloud occurrence as a function of altitude indicates that neither can obtain a complete picture of the vertical profile of cloud occurrence in this region.

Examination of the liquid phase cloud profiles shows a number of differences between the three datasets. Liquid phase cloud profiles for AWARE match well with the DARDAR profiles during November (Figure 3c) and December (Figure 3d), but match more poorly in January and October (Figure 3a and b). It is likely that November and December were dominated by optically-thin clouds that both datasets capture, while January and October were dominated by frequent frontal systems, that resulted in the large discrepancies between the satellite and ground–based measurements. Overall, neither the 2BCL5 or DARDAR datasets consistently agree with the liquid phase cloud reported by the AWARE dataset. Given the known weaknesses in the satellite datasets at detecting low–level cloud, this is expected. Ice-only phase cloud profiles are difficult to compare, due to both a lack of a reliable mixed phase cloud classification in the AWARE dataset and discrepancies in the definition of ice-only clouds in the satellite datasets.

### 3.3 2BCL5 and DARDAR cloud detections compared to AWARE

Figure 3 shows that both 2BCL5 and DARDAR underestimate cloud occurrence at low altitudes compared to AWARE observations, but is limited as it does not provide a direct comparison of individual profiles. To compare the individual profiles between the datasets, the frequency of cloud detections between 2BCL5, DARDAR, and AWARE for each pass over McMurdo Station during 2016 is examined. Cloud detections for the space–borne (S) and ground–based (G) observations are separated into three categories:

1. Where both the space–borne and ground–based observations identify cloud detections (The intersection of both the space–borne and ground–based observations is identified, $S \cap G$).

2. Where only the ground–based observations has a cloud detection (The intersection of the ground–based observations with the complement of the space–borne observations is identified, $S^c \cap G$).

3. Where only the space–borne observations has a cloud detection (The intersection of the space–borne observations with the complement of the ground–based observations is identified, $S \cap G^c$).

Figure 4 shows a comparison of the detection frequency between 2BCL5 and AWARE (a, d, g) and DARDAR and AWARE (b, e, h) for the three previously defined categories. This allows us to assess if one or both the space–borne and ground–based instruments detect cloud at a particular altitude. The detection frequency is defined as the proportion of the time across all passes where the underlying conditions between the two sets are satisfied. Differences in the detection frequency for each category are displayed in Figure 4 (c, f, i) to highlight the discrepancies between 2BCL5 and DARDAR.

Figure 4 a shows that above 1 km AWARE observations detect clouds that are not identified by the 2BCL5 dataset approximately 10% of the time. Below 1 km the AWARE dataset detects a greater amount of clouds than observed by 2BCL5, with a maximum difference of 53%. As such, 2BCL5 is unable to accurately detect low altitude clouds relative to ground-based observations. Conversely, Figure 4d shows that the 2BCL5 has observations undetected by AWARE 10% - 20% from near the surface to roughly 6.5 km. While cloud detections observed only by 2BCL5 at higher altitudes might be expected, it is surprising that 2BCL5 detects clouds that are not observed by AWARE at lower altitudes.

These results suggest either limitations in the AWARE dataset, differences between the satellite footprint and ground observations, or a potential issue with 2BCL5 falsely identifying clutter in the radar and/or lidar signals as cloud detections. Figure 4g shows that below 9 km the frequency of AWARE and 2BCL5 both detecting cloud increases until it peaks at 42% near 2 km after which a sharp decrease is observed.

Figure 4b compares the DARDAR and AWARE datasets and shows that above 1 km AWARE detects clouds unobserved in the DARDAR dataset approximately 10% of the time. Below 0.8 km the frequency where only AWARE observes a cloud detection rises to a peak of 44%. This likely indicates that both of the satellite datasets are unable to accurately observe clouds below 1 km. Figure 4e shows that between 1 and 7 km DARDAR detects clouds unobserved by AWARE roughly 10% - 20% of the time. Above 7 km the frequency reduces to below 10% as detections become sparse. Interestingly, below 1 km the frequency increases to 25% of the DARDAR overpasses identifying a cloud unobserved by AWARE. This either suggest instrumental limitations in the AWARE dataset or issues with DARDAR where false positives in the radar/lidar signals are detected. The latter hypothesis is more likely given the known weaknesses in the satellite datasets. Figure 4h shows that similar to 2BCL5, the frequency of both DARDAR and AWARE observing cloud increases at lower altitudes, peaking at 42% at an altitude of 2 km, followed by a decrease at lower altitudes.

While similar overall, both 2BCL5 and DARDAR display some differences in how their cloud detections match with AWARE. Above 1 km, DARDAR and 2BCL5 show good agreement, while below 1 km there is a large difference between the two datasets. Figure 4c shows that below 1 km cases where only AWARE detects a cloud is 10% - 15% greater for 2BCL5 than DARDAR. This is mirrored by Figure 4i where below 1km, DARDAR observes a greater amount of cloud detections than 2BCL5, which are also observed

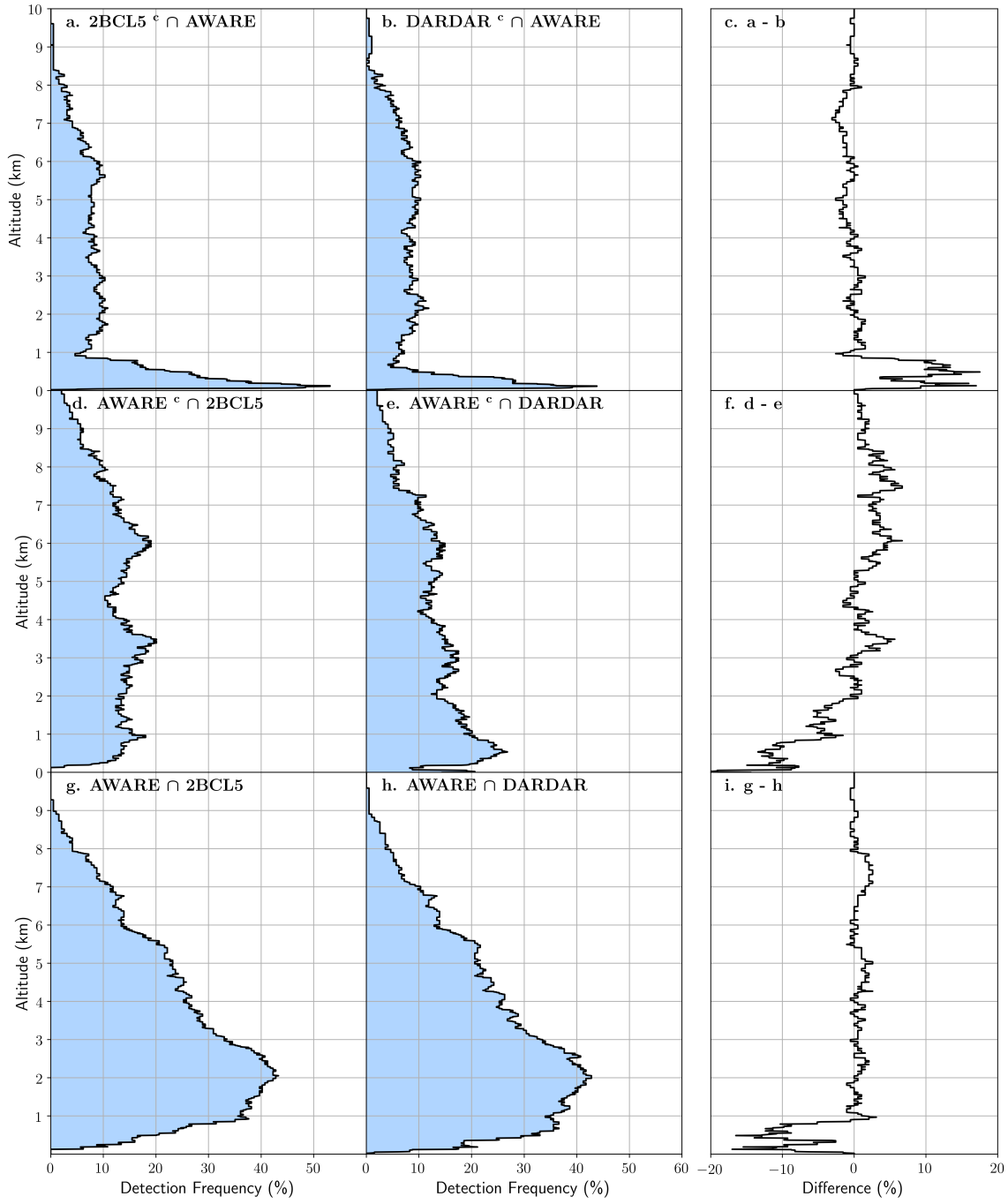


**Figure 4.** Detection frequency as a function of altitude for (a, d, g) 2BCL5 and AWARE and (b, e, h) DARDAR and AWARE showing where only the ground–based (a, b), space–borne (d, e) or both (g, h) datasets have cloud detections. Differences in the detection frequency for each categorisation are also displayed (c, f, i) to highlight the anomaly between 2BCL5 and DARDAR.

by AWARE. This result suggests that DARDAR agrees better with AWARE than 2BCL5 below 1 km, while the two have comparable detectability elsewhere. However, this could be a result of DARDAR having greater cloud occurrences than 2BCL5 below 1 km, rather than an improved match with AWARE. Figure 4h shows that below 1 km, DARDAR

has a greater amount of cloud detections where AWARE does not observe any cloud relative to 2BCL5. This probably indicates that DARDAR is classifying noise in the radar/lidar signals close to the ground as clouds, resulting in a 10% - 15% larger false positive rate than 2BCL5.

### 3.4 Ratios between satellite and ground–based detected cloud occurrences

The 180 satellite overpasses in which 2BCL5, DARDAR, and AWARE all detected clouds were examined and spatially and temporally colocated atmospheric profile from the different datasets were compared. Figure 5a and b show the ratio of 2BCL5 and DARDAR cloud occurrence to the AWARE cloud occurrence for each co-location, respectively. Figure 5 a and b also show the median value at each altitude for both 2BCL5/AWARE (red) and DARDAR/AWARE (black). The ratio between 2BCL5 and DARDAR is displayed in Figure 5c with the median curve illustrated in blue.

Figure 5a shows that the median ratio of cloud occurrence between 2BCL5 and AWARE match well between 1.5 and 4.5 km, with relative differences less than 10%. However, there is a large spread of values at this altitude range, which indicates that while it is common for the two datasets to detect similar cloud profile structures, this is not always the case. Below 1.5 km the median ratio shows that 2BCL5 underestimates cloud occurrence compared to the AWARE dataset. This ratio decreases to a local minimum of 0.24 at 0.8 km, corresponding to an underestimation in 2BCL5, identifying that 2BCL5 only observes 24% of the cloud occurrence relative to the AWARE observations. Below 0.8km the detectability of 2BCL5 improves slightly, with 2BCL5 observing 37% of AWARE cloud occurrence at 0.5 km, before steadily decreasing below 0.25 km. Above 4.5 km the two datasets also disagree, but with AWARE likely underestimating compared to 2BCL5. As the altitude increases the median ratio fluctuates up to an altitude of around 7.5 km and then steadily increases until AWARE observes between 37%–61% of cloud observed by 2BCL5. Above this altitude there is little consistency as the AWARE instruments have difficulties in detecting clouds at this altitude.

Figure 5b shows a limited agreement between DARDAR and AWARE. Between 3 and 5 km there is good agreement (within 10%). Extending this range to between 1.5 and 6 km there is poorer agreement with differences of up to 20%. Similar to the 2BCL5 dataset, DARDAR starts to consistently underestimate cloud occurrence compared to AWARE below 1.5 km. The median drops to 0.37 at 0.5 km. This likely corresponds to limitations in DARDAR, which only observes 37% of cloud occurrence detected by AWARE at that altitude. As for the comparison with 2BCL5, the ratio between DARDAR and AWARE cloud occurrence decreases towards the surface. Above 6 km the two datasets also disagree, with AWARE underestimating cloud occurrence compared to the DARDAR dataset. The median ratio fluctuates between 6 - 8 km, ranging from near even to altitudes where AWARE has 37% of the DARDAR occurrences. At higher altitudes the ratio changes rapidly as only a few profiles are available for the statistical analysis.

Figure 5c shows that DARDAR consistently underestimates cloud occurrence compared to 2BCL5 above 1 km with only shows a few instances above 1 km where DARDAR detects more cloud. This is possibly a result of the lower cloud occurrences in DARDAR above 1 km (see Figure 2). Below 1 km there is clearly a wider range of ratios and we might expect that DARDAR would show greater cloud occurrence below 1 km compared to 2BCL5 based on (Figure 4i). However, it is clear from these ratios that DARDAR may actually have a greater frequency of false cloud detections than 2BCL5.

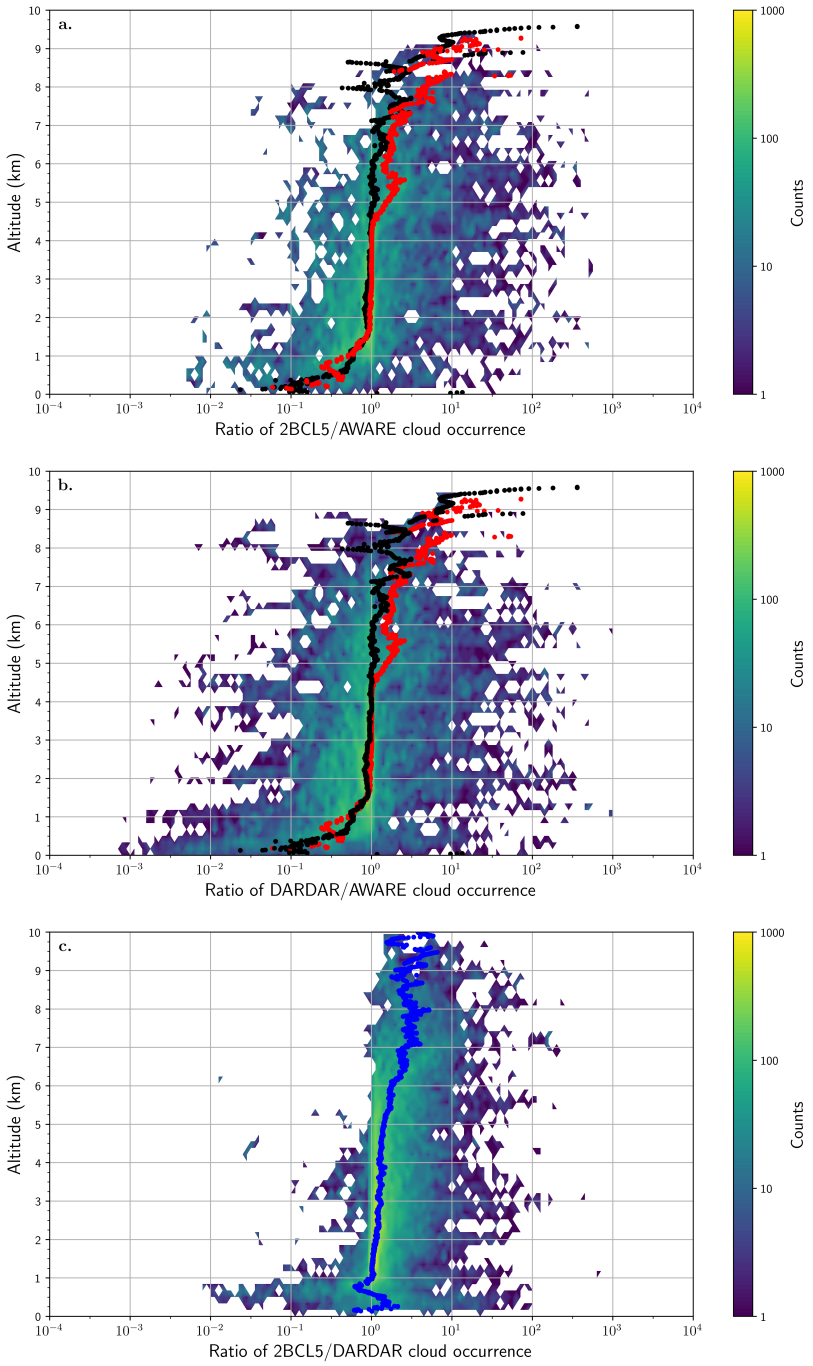


**Figure 5.** The ratio between satellite and ground–based cloud occurrence at different altitudes, for (a) 2BCL5/AWARE (b) DARDAR/AWARE and (c) 2BCL5/DARDAR. Both (a) and (b) display the medians for 2BCL5/AWARE (red) and DARDAR/AWARE (black) while the median for 2BCL5/DARDAR is shown on (c) in blue.

### 3.5 Statistical evaluation of the 2BCL5, DARDAR and AWARE distributions of cloud occurrence

The ratios of cloud occurrence rates clearly show distinct behaviours over different altitude ranges. In order to quantify these differences, statistical tests are applied

to the distributions of cloud occurrence in 1 km altitude bins. Each of these regions are examined using a t-test and a Kolmogorov–Smirnov (K-S) test. The t-test is used to analyze the differences in the means of cloud occurrence distributions between the 2BCL5 and AWARE and the DARDAR and AWARE datasets. The K-S test is used to compare whether the cloud occurrence distributions of 2BCL5 and AWARE or DARDAR and AWARE are statistically distinct from one another. The t-test produces a t-statistic (t), where a higher t-value indicates greater differences between the means of the distributions. The K-S test produces a K-S statistic (D), which evaluates the distance between the two cumulative distribution functions with a higher D-value corresponding to a greater distance. Both tests also produce a p-value, indicating the significance of the test statistics. If the p-value is less than a predefined significance level ($\alpha$), then the corresponding test statistics are considered statistically significant and the null hypothesis can be rejected. The significance level is chosen to be 5% and the results of the statistical tests are displayed in Figure 6. Simply put if a p-value is above the significance level it implies the satellites datasets agree with AWARE, while if it is below they are distinct from AWARE.

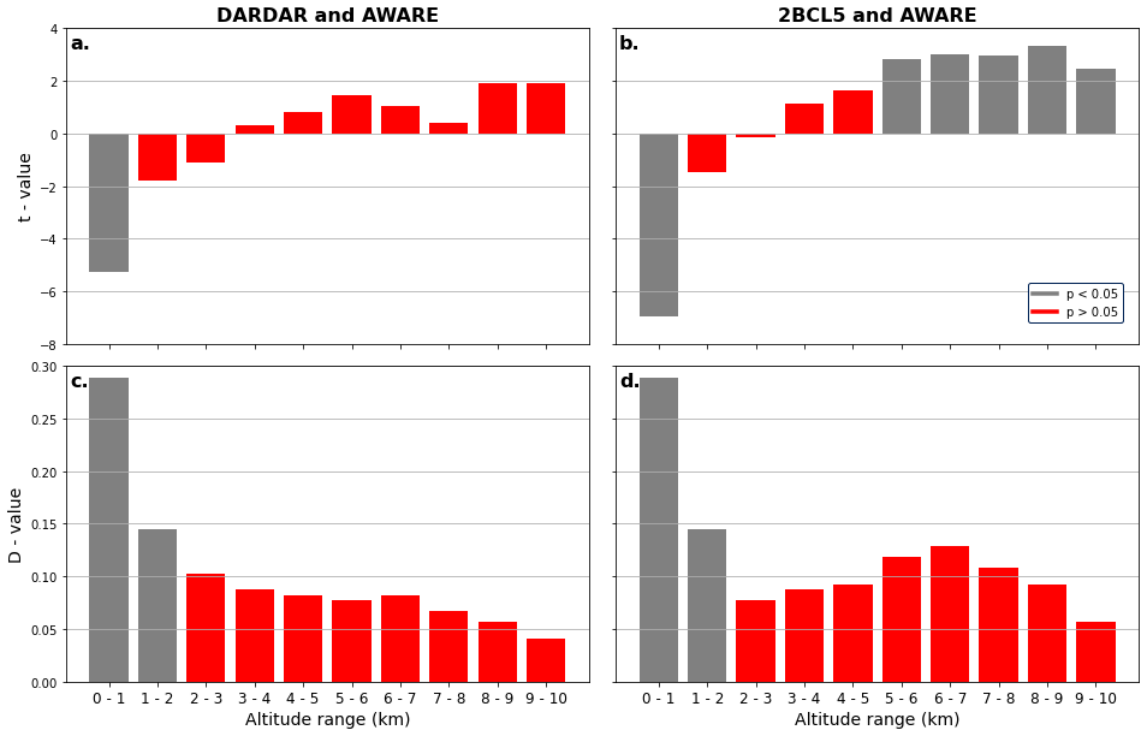


**Figure 6.** Results of the (a, b) t-test and (c, d) K-S test comparing the means and distributions of (a, c) DARDAR and AWARE and (b, d) 2BCL5 and AWARE. Red bars indicate where the p-value is less than the significance level, $\alpha = 0.05$.

Analysing the low level cloud between 0 and 1 km, the t-test and K-S test show that both the means and distributions of 2BCL5 and DARDAR compared to AWARE are statistically distinct. The largest t-values over this region are -7.0 between 2BCL5 and AWARE and -5.2 between DARDAR and AWARE. This indicates that the means of these cloud occurrences are very different in both cases. The D-values in this region are also large. Between 1 - 2 km, the K-S test indicates that the distributions of 2BCL5 and DARDAR are statistically distinct compared to AWARE, while the t-test shows that the means cannot be considered different from AWARE. Between 2 - 5 km, both 2BCL5

and DARDAR match well with AWARE, as both tests show that the means and distributions are statistically distinct. However, above 5 km the t-test shows drastically different results for the 2BCL5 data. The results of the t-test show that the means of the distributions for the 2BCL5 and AWARE datasets cannot be considered to be drawn from the same distribution, while the DARDAR and AWARE values continue to show that the means are statistically distinct. The K-S test continues to show show results above the significance threshold for both 2BCL5 and DARDAR, although the 2BCL5 D-values are clearly larger over this region. Given the relatively lower sensitivity of the AWARE data over this region, these results should be interpreted cautiously.

Over the entire altitude range the DARDAR cloud occurrence distributions match better to the AWARE data than the 2BCL5 based on both t and D values. The largest differences are seen above 5km where the t-tests consistently produce different results. This may seem to contradict the results that are shown in Figure 5, however this is due to differences in how these results should be interpreted. The statistics show that the underlying cloud occurrence distributions of DARDAR agree better with AWARE than 2BCL5 does. However, the ratio analysis shows us that when specific cases are examined the 2BCL5 data performs better. This implies that DARDAR might outperform 2BCL5 relative to AWARE in the statistical aggregate, but when looking at specific times and locations 2BCL5 generally matches better.

### 3.6 Cloud occurrence as a function of temperature

To further compare the cloud phases in the 2BCL5, DARDAR, and AWARE datasets, cloud occurrence was derived as a function of temperature. Temperature information was taken from twice-daily measurements taken from radiosondes launched at McMurdo Station, as well as the ECMWF-AUX temperature data. Figure 7 shows the normalised occurrence of cloud phase at each temperature for the three datasets examined, using both the ground–based and reanalysis temperature information.

Figure 7a shows 2BCL5 cloud occurrence identified relative to radiosonde temperature data. At temperatures above -12 °C, supercooled water dominates, but its occurrence quickly falls off as the proportions of mixed and ice phase cloud increases at lower temperatures. Ice phase clouds dominate occurrence at temperatures lower than -35 °C. However, mixed phase clouds are identified at temperatures down to -60 °C, which is clearly unphysical. This pattern matches well with Figure 7b, which uses the ECMWF-AUX measurements instead of the radiosondes. Thus, the unphysical classification can not be attributed to differences between the ECMWF-AUX data and the corresponding AWARE radiosonde measurements. Figures 7c and d display the DARDAR temperature based cloud occurrence. The DARDAR results identify that apart from a large presence of liquid phase clouds above -10 °C, ice phase clouds dominate. However, small amounts of mixed and liquid phase cloud are present down to temperatures of -43 °C, which again is unphysical. Once again, the ECMWF-AUX temperature output shows reasonable agreement with the ground–based temperature.

Figure 7e shows the AWARE cloud occurrence for different phases using the AWARE radiosonde measurements as the temperature reference. Most of the AWARE cloud detections are associated with the 'unknown' phase, highlighting a clear limitation of the AWARE data. Liquid phase clouds are detected in relatively small fractions down to a temperature of approximately -35 °C. Ice phase cloud occurrence (detected with the HSRL) is more common than liquid and unknown phases at the higher temperatures but falls off significantly at lower temperatures, because of increasingly large amounts of unknown phase cloud detections. A secondary peak of ice cloud at -60 °C which is partially associated with polar stratospheric cloud detections in tropospheric cloud-free periods. This matches observations in Figure 3 where the ability to classify phase falls off as altitude increases (and conversely the temperature decreases), which is clearly due to the atten-

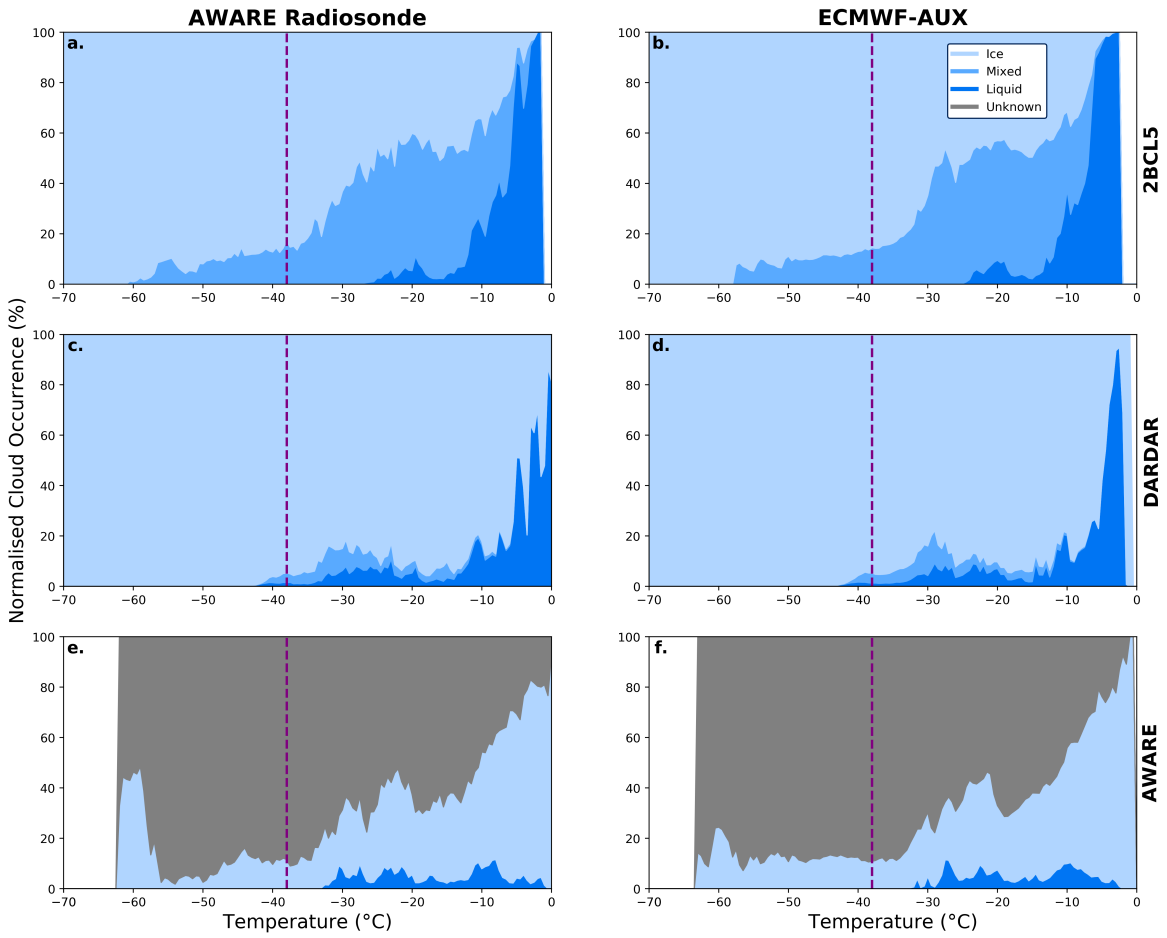


**Figure 7.** Normalised cloud occurrences from Figure 3 as a function of temperature for (a - b) 2BCL5 (c - d) DARDAR and (e - f) AWARE. 2BCL5 and DARDAR cloud occurrences are split into ice, mixed and liquid phases, and AWARE cloud occurrence into the ice, liquid and 'unknown' phase classes (see text for details). White space indicates where cloud is undetected and the dashed line indicates the edge of the homogeneous freezing regime at -38 °C.

uation of the HSRL signal by low-level cloud. Figure 7f again shows a good match between the ECMWF-AUX and AWARE radiosonde temperature information, although the peak in the ice phase cloud at -60 °C is weaker.

Cloud phase data from AWARE matches well with the boundary of the homogeneous freezing regime at -38 °C. There is some uncertainty in this result due to the majority of the clouds here being unclassified. The overall lack of liquid phase detections in AWARE does suggest that some of the unknown phase detections are associated with supercooled water. In both 2BCL5 and DARDAR, cloud measurements are found outside the physical limits defined by the homogeneous freezing threshold. For clouds classified as mixed phase by 2BCL5, 13.3% occur at temperatures below the -38 °C isotherm in the AWARE radiosonde measurements, and 13.8% for the ECMWF-AUX data product. For the DARDAR dataset 1.1% of cloud classified as liquid phase and 5.7% of clouds classified as mixed phase occur below the -38 °C isotherm for the AWARE radiosonde measurements. When using ECMWF-AUX data as a reference 1.3% of clouds classified as liquid phase and 6.6% of clouds classified as mixed phase occur below the -38 °C isotherm.

This coincident temperature analysis shows that DARDAR also incorrectly classifies mixed phase cloud within the homogeneous freezing regime, albeit to a smaller extent than 2BCL5.

## 4 Discussion

Figure 3 shows that cloud occurrence for all phases have maximum values between 1.5 and 3 km for both 2BCL5 and DARDAR. Below this level cloud occurrence falls off rapidly with low cloud occurrence below 1 km for 2BCL5 and 0.5 km for DARDAR. AWARE ground-based observations display a maximum in cloud occurrence at a slightly lower altitude (between 1 and 2.5 km), but also show larger cloud occurrences at lower levels. Above the maxima, AWARE cloud occurrence tends to fall off faster than the 2BCL5/DARDAR data. As the lidar signal used within the AWARE dataset is often attenuated above 4 km, detection of high level clouds is likely underestimated. While the KAZR can still detect many of these clouds, it struggles to detect high level cirrus with small optical depths (Sassen & Khvorostyanov, 1998). Therefore neither 2BCL5, DARDAR or AWARE appears to be able to observe the complete vertical structure of clouds. Thus, to obtain the full picture, a combination of ground–based and space–borne measurements are needed. However, merging these datasets is not straight forward because of the large disparities at nearly all altitudes. Comparisons of cloud occurrences in Figure 3 can be compared with previous work investigating cloud phase using four years of 2BCL5 data over the Ross Sea and Ross Ice Shelf detailed in Jolly et al. (2018). The results of their study show reasonable agreement with the results of the 2016 2BCL5 data obtained in this study. This suggests that the 2016 2BCL5 data is representative of the long-term cloud patterns observed in this region.

The comparisons between the vertical profiles of cloud occurrence at AWARE, 2BCL5, and DARDAR establish three distinct regions; a region where the satellite likely underestimates cloud close to the ground, a region where the ground–based instruments likely underestimate at higher altitudes, and a region of approximate agreement in between. The statistical analysis in Figure 6 shows both 2BCL5 and DARDAR are substantially different from AWARE at low altitudes. It might be expected that DARDAR cloud occurrence would match better with the AWARE dataset than the 2BCL5 because DARDAR observes higher cloud occurrences below 1 km. However, this is not the case, as the altitude at which the satellite datasets begin to deviate from AWARE is essentially the same (see Figure 5). Thus, we conclude that even though DARDAR observes more clouds below 1 km than 2BCL5, it does not appear to be detecting low–level clouds more reliably than the 2BCL5 dataset. Instead, DARDAR appears to be detecting false positives in the lidar/radar signals by incorrectly interpreting noise close to the ground as clouds.

These results are generally consistent with conclusions from previous studies (e.g., Protat et al., 2014; Blanchard et al., 2014; Y. Liu et al., 2017; Alexander & Protat., 2018), which show underestimations of satellite–based cloud observations compared to ground–based observation. For example, Alexander and Protat. (2018) found underestimation of DARDAR cloud observations by a factor of three between 0.2 - 1 km compared with a ground–based lidar. However, their study only included low level optically-thin single cloud layers where both the ground based lidar and DARDAR masks could detect the cloud top and cloud base (lidar signal transmitted through cloud top). Y. Liu et al. (2017) also found that space–borne observations, such as the 2B-GEOPROF-lidar dataset (Mace et al., 2009), begin to drop off significantly below 1 km similar to this study. In particular, they note that below 0.5 km satellite–based observations detect 25–40% fewer clouds than observed by a ground–based lidar. One study by Mioche et al. (2015) found that over the Svalbard region in the Arctic satellite observations overestimates cloud occurrence below 2 km compared to surface based micropulse lidar observations. However, the authors associated this overestimation with the short duration of their dataset. Previous work (e.g., Bodas-Salcedo et al., 2012; Schuddeboom et al., 2018; Kuma et al., 2020)

has shown climate models underestimate low–level cloud compared to satellite datasets. Given that the satellite measurements in this paper are shown to underestimate low–level cloud occurrence compared to AWARE observations, the magnitude of these model errors could be larger than previously identified.

For the mid-altitude region, the median ratio shows that 2BCL5 and AWARE are in good agreement between 1.5 and 4.5 km and for the most part shows an equal amount of cloud (within 10%). DARDAR shows a good level of agreement with AWARE between 1.5 and 6 km, extending further than 2BCL5, but the match is weaker (within 20%). This match between DARDAR and AWARE extending to a greater altitude is likely because both AWARE and DARDAR observe fewer clouds than 2BCL5 at these heights. The results of the statistical tests (Figure 6) show that both DARDAR and AWARE and 2BCL5 and AWARE match well between 2 and 5 km, suggesting that the underlying cloud occurrence distributions are well captured in this region.

At altitudes greater than 6 km, the median ratio of cloud occurrence shows that both DARDAR and 2BCL5 detect more clouds than AWARE, but this is probably due to AWARE being unable to detect clouds rather than the satellite signals being dominated by false positives. The ratio between the satellite and ground–based measurements (Figure 5a/b) is variable at high altitudes and close to the ground because not all passes can be compared at all heights. Figure 4c and Figure 4f show that above 7 km the comparisons between the two satellite datasets can only be made 10% of the time as the detection frequency decreases. This suggests that the underestimation of AWARE at high altitudes relative to 2BCL5 (Figure 5a) and DARDAR (Figure 5b) is potentially worse than stated. Below 1 km a similar pattern is observed where the amount of detected cloud-containing profiles that can be compared drops as the satellites are unable to observe clouds detected by AWARE. The t-tests in Figure 6 show divergent results for 2BCL5 and DARDAR over this region, however due to the limitations with the AWARE dataset these should be interpreted with caution.

Figure 7 shows that DARDAR and 2BCL5 observe mixed and liquid phase cloud regions outside theoretical temperature thresholds using both the AWARE radiosonde or ECMWF-AUX temperature data. However, the 2BCL5 data product classifies cloud phase incorrectly more often than the DARDAR product despite the fact that both 2BCL5 and DARDAR use the same ECMWF-AUX temperature data. Differences in how 2BCL5/DARDAR assign phase to their cloud detections must therefore explain why their phase determinations are different. For 2BCL5, each cloud layer with a distinct top and bottom is assigned a single phase. DARDAR classifies each pixel in a cloud layer separately, so a cloud layer identified by 2BCL5 might have multiple classifications given by DARDAR. This could allow 2BCL5 to identify mixed phase above the -38 °C isotherm altitude. In addition, mixed phase clouds are defined by the 2BCL5 product as a combination of ice and supercooled water existing in the cloud layer, resulting in the whole cloud being classified as a mixed phase cloud. If a mixed phase cloud exists at the cloud base where temperatures are between 0 °C and -38 °C, 2BCL5 would also assign a mixed phase to the cloud top where temperatures are above -38 °C and mixed phase cloud will not be present.

Due to a large proportion of the AWARE dataset clouds being classified as an "unknown" phase, it becomes difficult to draw comparisons between cloud phases for the satellite– and the ground–based datasets and to evaluate the reliability of liquid or mixed-phase detections by the satellite retrievals within the heterogeneous freezing regime. 2BCL5 uses a process primarily driven by the temperature of the cloud top and cloud base, but also uses a temperature dependent radar reflectivity ($Z_e$) threshold and an integrated attenuated backscattering coefficient (see Zhang et al., 2010). This splits the cloud into liquid, ice and mixed phase cloud containing a combination of ice and liquid. Contrastingly, DARDAR uses the strength of the lidar backscatter signal to locate any attenuating high backscatter layers. DARDAR then attempts to classify these layers based on temperature, horizontal extent of layer, thickness, reflectivity, and altitude. The algo-

rithms used on the AWARE dataset use particulate backscatter cross-section and linear depolarisation ratio to split the lidar observations of cloud into liquid and ice cloud. Due to attenuation of their lidar instrument, much of their cloud observations can not be reliably classified and are instead classified as unknown. In order to draw better comparisons between the phases, consistent processing algorithms with high fidelity, which could simultaneously consider satellite and ground-based measurement limitations, would be needed to be applied to the raw radar/lidar measurements rather than trying to match separately processed products together. Another possibility is to use instrument simulators to help to interpret the different data relative to model data (Kuma et al., 2020b).

## 5 Conclusions

In this study vertical profiles of cloud occurrence and cloud phase for the 2BCL5 and DARDAR satellite data products are compared to ground–based AWARE observations taken during 2016. An assessment of the global distributions of 2BCL5 and DARDAR cloud occurrence found key differences between the two datasets quantification of low-level clouds and cloud phase. These differences are greatest for low–level clouds over high southern latitudes, providing a strong motivation for a detailed investigation of vertical cloud occurrence using ground–based measurements from the AWARE campaign over McMurdo Station in Antarctica.

Satellite observations for both 2BCL5 and AWARE show an underestimation of cloud occurrence below 1.5 km compared to ground–based AWARE observations, with both 2BCL5 and DARDAR observing 37% of clouds detected at AWARE at an altitude of 0.5 km. Conversely, at altitudes greater than 6 km the AWARE dataset shows an underestimation of cloud occurrence compared to the 2BCL5 and DARDAR datasets, likely attributed to the attenuation of the HSRL signal by low-level clouds and lower KAZR detectability at long ranges, where the radar volumes are significantly larger. In between these altitude ranges, there was a good agreement between AWARE and the satellite–based datasets.

Below 1 km DARDAR observes a greater cloud occurrence than 2BCL5, and relatively lower occurrence at higher altitudes. Even though DARDAR observes more cloud below 1 km than 2BCL5, when compared to coincident and contemporaneous AWARE detections, it is not more reliable than the 2BCL5 dataset; DARDAR detects clouds that are not detected in the AWARE dataset between 20–25% of the time below 1 km compared to 10–15% for 2BCL5. This indicates that the higher DARDAR cloud occurrence below 1 km is likely associated with false detections where DARDAR is likely incorrectly classifying ground clutter or from the radar signal, or attenuated lidar retrievals, as cloud.

2BCL5 and DARDAR estimates of cloud phase were also found to deviate from physical constraints set by the temperatures at which a combination of ice and supercooled water should exist. 2BCL5 shows 13.3% (13.8%) of mixed phase clouds occurring at temperatures within the homogeneous freezing regime below -38 °C, with mixed-phase observations down to a temperature of -60 °C (-58 °C) in the case where radiosonde (ECMWF-AUX) temperature data are used. DARDAR shows 5.7% (6.6%) of mixed phase and 1.1% (1.3%) of liquid phase clouds within the homogeneous freezing regime down to a temperature of -43 °C for radiosonde (ECMWF-AUX) data.

Overall, the results presented here emphasize the need for a combination of ground–based and space–borne measurements to fully characterise cloud structure. This may be particularly important over the Southern Ocean and Antarctica given the large disparities observed in low-level cloud in this region.

**Acknowledgments**

The 2B-CLDCLASS-LIDAR and ECMWF-AUX products were obtained from the CloudSat Data Processing Center (http://www.cloudsat.cira.colostate.edu/). DARDAR data products were downloaded from the ICARE Data and Service Center (http://www.icare.univ-lille1.fr). The AWARE data used in this study are available in the ARM data archive (http://www.archive.arm.gov). We would like to acknowledge funding from the Deep South National Science Challenge which has partially supported this research. I.S. was supported by the DOE grants DE-SC0017981. and DE-SC0018046.

## References

Alexander, S. P., & Protat., A. (2018). Cloud properties observed from the surface and by satellite at the northern edge of the southern ocean. *Journal of Geophysical Research: Atmospheres*, *123*(1), 443-456. doi: 10.1002/2017jd026552

Blanchard, Y., Pelon, J., Eloranta, E. W., Moran, K. P., Delanoë, J., & Sèze, G. (2014). A synergistic analysis of cloud cover and vertical distribution from a-train and ground-based sensors over the high arctic station eureka from 2006 to 2010. *Journal of Applied Meteorology and Climatology*, *53*(11), 2553-2570. doi: 10.1175/jamc-d-14-0021.1

Bodas-Salcedo, A., Hill, P., Furtato, K., Williams, K., Field, P., Manners, J., & Hyder, P. (2016). Large contribution of supercooled liquid clouds to the solar radiation budget of the southern ocean. *Journal of Climate*, *29*(11), 4213-4228. doi: 10.1175/jcli-d-15-0564.1

Bodas-Salcedo, A., Williams, K., Field, P., & Lock, A. (2012). The surface downwelling solar radiation surplus over the southern ocean in the met office model: The role of midlatitude cyclone clouds. *Journal of Climate*, *25*, 7467–7486. doi: 10.1175/jcli-d-11-00702.1

Bodas-Salcedo, A., Williams, K. D., Ringer, M. A., Beau, I., Cole, J. N. S., Dufresne, J. L., ... Yokohata, T. (2014). Origins of the solar radiation biases over the southern ocean in cfmip2 models. *Journal of Climate*, *27*, 41-56. doi: 10.1175/JCLI-D-13-00169.1

Ceccaldi, M., Delanoë, J., Hogan, R. J., Pounder, N. L., Protat, A., & Pelon, J. (2013). From cloudsat-calipso to earthcare: Evolution of the dardar cloud classification and its comparison to airborne radar-lidar observations. *Journal of Geophysical Research: Atmospheres*, *118*(14), 7962-7981. doi: 10.1002/jgrd.50579

Ceppi, P., Hwang, Y.-T., Frierson, D. M., & Hartmann, D. L. (2012). Southern hemisphere jet latitude biases in cmip5 models linked to shortwave cloud forcing. *Geophysical Research Letters*, *39*(19). doi: 10.1029/2012GL053115

Cess, R. D. (1990). General circulation model intercomparisons for understanding climate. long-term monitoring of the earth's radiation budget. *Journal of Geophysical Research - Atmospheres*, *95*(D10), 16601-16615. doi: 10.1117/12.21359

Chubb, T. H., Jensen, J. B., Siems, S. T., & Manton, M. J. (2013). In situ observations of supercooled liquid clouds over the southern ocean during the hiaper pole-to-pole observation campaigns. *Geophysical Research Letters*, *40*(19), 5280-5285. doi: 10.1002/grl.50986

Coggins, J., A., M., & Jolly, B. (2014). Synoptic climatology of the ross ice shelf and ross sea region of antarctica: k-means clustering and validation. *nternational Journal of Climatology*, *34*(7), 2330-2348. doi: 10.1002/joc.3842

Delanoë, J., & Hogan, R. J. (2010). Combined cloudsat-calipso-modis retrievals of the properties of ice clouds. *Journal of Geophysical Research*, *115*. doi: 10.1029/2009jd012346

Eloranta, E. (2005). High spectral resolution lidar. in lidar: Range-resolved optical remote sensing of the atmosphere. *New York: Springer New York.*. doi: 10

.1007/0-387-25101-4_5

Haynes, J. M., Jakob, C., Rossow, W. B., Tselioudis, G., & Brown, J. (2011). Major characteristics of southern ocean cloud regimes and their effects on the energy budget. *Journal of Climate*, *24*(19), 5061-5080. doi: 10.1175/2011jcli4052.1

Hu, Y., Winker, D., Vaughan, M., Lin, B., Omar, A., Trepte, C., & Flittner, D. (2009). Calipso/caliop cloud phase discrimination algorithm. *Journal of Atmospheric and Oceanic Technology*, *26*(11), 2293-2309. doi: 10.1175/2009jtecha1280.1

Hwang, Y., & Frierson, D. (2013). Link between the double-intertropical convergence zone problem and cloud biases over the southern ocean. *Proceedings of the National Academy of Sciences*, *110*(13), 4935-4940. doi: 10.1073/pnas.1213302110

Hyder, P., Edwards, J., Allan, R., Hewitt, H., Bracegirdle, T., Gregory, J., ... Belcher, E. (2018). Critical southern ocean climate model biases traced to atmospheric model cloud errors. *Nature Communications*, *9*(1), 3625. doi: 10.1038/s41467-018-05634-2

Jolly, B., Kuma, P., McDonald, A., & Parsons, S. (2018). An analysis of the cloud environment over the ross sea and ross ice shelf using cloudsat/calipso satellite observations: The importance of synoptic forcing. *Atmospheric Chemistry and Physics*, *18*(13), 9723-9739. doi: 10.5194/acp-18-9723-2018

Kay, J., Hillman, B., Klein, S., Zhang, Y., Medeiros, B., Pincus, R., ... T., A. (2012). Exposing global cloud biases in the community atmosphere model (cam) using satellite observations and their corresponding instrument simulators. *Journal of Climate*, *25*(15), 5190-5207. doi: 10.1175/jcli-d-11-00469.1

Kay, J., Wall, C., Yettella, V., Medeiros, B., Hannay, C., Caldwell, P., & Bitz, C. (2016). Global climate impacts of fixing the southern ocean shortwave radiation bias in the community earth system model (cesm). *Journal of Climate*, *29*(12), 4617-4636. doi: 10.1175/jcli-d-15-0358.1

Kuma, P., McDonald, A., Morgenstern, O., Alexander, S., Cassano, J., Garrett, A., ... Williams, J. (2020). Evaluation of southern ocean cloud in the hadgem3 general circulation model and merra-2 reanalysis using ship-based observations. *Atmospheric Chemistry and Physics Discussions*, *20*(11), 6607-6630. doi: 10.5194/acp-2019-201

Kuma, P., McDonald, A. J., Morgenstern, O., Querel, R., Silber, I., & Flynn, C. J. (2020b). Ground-based lidar processing and simulator framework for comparing models and observations. *Geoscientific Model Development Discussions*, *2020*, 1-45. Retrieved from `https://doi.org/10.5194/gmd-2020-25` (in review) doi: 10.5194/gmd-2020-25

Lamb, D., & Verlinde, J. (2011). Nucleation. In *Physics and chemistry of clouds.* (p. 298-318). New York: Cambridge University Press.

Listowski, C., Delanoë, J., Kirchgaessner, A., Lachlan-Cope, T., & King, J. (2018). Antarctic clouds, supercooled liquid water and mixed-phase investigated with dardar: Geographical and seasonal variations. *Atmospheric Chemistry and Physics*, *19*(10). doi: 10.5194/acp-19-6771-2019

Liu, Y., Shupe, M. D., Wang, Z., & Mace, G. (2017). Cloud vertical distribution from combined surface and space radar–lidar observations at two arctic atmospheric observatories. *Atmospheric Chemistry and Physics*, *17*(9), 5973-5989. doi: 10.5194/acp-17-5973-2017

Liu, Z. (2009). The calipso lidar cloud and aerosol discrimination: Version 2 algorithm and initial assessment of performance. *Journal of Atmospheric and Oceanic Technology*, *26*(7), 1198-1213. doi: 10.1175/2009jtecha1229.1

Lubin, D., Zhang, D., Silber, I., Scott, R. C., Kalogeras, P., Battaglia, A., ... Vogelmann, A. M. (2020, 02). AWARE: The Atmospheric Radiation Measurement (ARM) West Antarctic Radiation Experiment. *Bulletin of the American Meteorological Society*. Retrieved from `https://doi.org/10.1175/`

BAMS-D-18-0278.1 doi: 10.1175/BAMS-D-18-0278.1

Mace, G., Zhang, Q., Vaughan, M., Marchand, R., Stephens, G., Trepte, C., & Winker, D. (2009). A description of hydrometeor layer occurrence statistics derived from the first year of merged cloudsat and calipso data. *Journal of Geophysical Research*, *114*. doi: 10.1029/2007jd009755

Marchand, R., Mace, G., Ackerman, T., & G., S. (2008). Hydrometeor detection using cloudsat—an earth-orbiting 94-ghz cloud radar. *Journal of Atmospheric and Oceanic Technology*, *25*, 519-533. doi: 10.1175/2007JTECHA1006.1

Marshall, J., & Plumb, R. A. (2008). *Atmosphere, ocean and climate dynamics: An introductory text.* Elsevier.

Mason, S., Fletcher, J. K., Haynes, J. M., Franklin, C., Protat, A., & Jakob, C. (2015). A hybrid cloud regime methodology used to evaluate southern ocean cloud and shortwave radiation errors. *Journal of Climate*, *28*, 6001-6018. doi: 10.1175/JCLI-D-14-00846.1

Matus, A. V., & L'ecuyer, T. S. (2017). The role of cloud phase in earth's radiation budget. *Journal of Geophysical Research: Atmospheres*, *122*(5), 2559-2578. doi: 10.1002/2016jd025951

McCoy, D., Hartmann, D., & Grosvenor, D. (2014). Observed southern ocean cloud properties and shortwave reflection. part i: Calculation of sw flux from observed cloud properties. *Journal of Climate*, *27*(23), 8836-8857. doi: 10.1175/jcli-d-14-00287.1

Mioche, G., Jourdan, O., Ceccaldi, M., & Delanoë, J. (2015). Variability of mixed-phase clouds in the arctic with a focus on the svalbard region: A study based on spaceborne active remote sensing. *Atmospheric Chemistry and Physics*, *15*(5), 2445-2461. doi: 10.5194/acp-15-2445-2015

Morrison, A. E., Siems, S. T., & Manton, M. J. (2011). A three-year climatology of cloud-top phase over the southern ocean and north pacific. *Journal of Climate*, *24*(9), 2405-2418. doi: 10.1175/2010jcli3842.1

Nayak, M. (2012). Cloudsat anomaly recovery and operational lessons learned. *SpaceOps 2012 Conference*. doi: 10.2514/6.2012-1295798.

Partain, P. (2007). *Cloudsat ecmwf-aux auxiliary data process description and interface control document.* Retrieved from http://www.cloudsat.cira.colostate.edu/sites/default/files/products/files/ECMWF-AUX_PDICD.P_R04.20070718.pdf

Protat, A., Armstrong, A., Haeffelin, M., Morille, Y., Pelon, J., Delanoë, J., & Bouniol, D. (2006). Impact of conditional sampling and instrumental limitations on the statistics of cloud properties derived from cloud radar and lidar at sirta. *Geophysical Research Letters*, *33*(11). doi: 10.1029/2005gl025340

Protat, A., Delanoë, J., O'Connor, E., & L'Ecuyer, T. (2010). The evaluation of cloudsat and calipso ice microphysical products using ground-based cloud radar and lidar observations. *Journal of Atmospheric and Oceanic Technology*, *27*(5), 793-810. doi: 10.1175/2009jtecha1397.1

Protat, A., Young, S. A., Mcfarlane, S. A., L'Ecuyer, T., Mace, G. G., Comstock, J. M., ... Delanoë, J. (2014). Reconciling ground-based and space-based estimates of the frequency of occurrence and radiative effect of clouds around darwin, australia. *Journal of Applied Meteorology and Climatology*, *53*(2), 456-478. doi: 10.1175/jamc-d-13-072.1

Rossow, W. B., & Schiffer, R. A. (1999). Advances in understanding clouds from isccp. *Bulletin of the American Meteorological Society*, *80*(11), 2261-2287. doi: 10.1175/1520-0477(1999)0802.0.co;2.

Salomonson, V., Barnes, W., Xiong, J., Kempler, S., & Masuoka, E. (2002). An overview of the earth observing system modis instrument and associated data systems performance. *IEEE International Geoscience and Remote Sensing Symposium.*. doi: 10.1109/igarss.2002.1025812

Sassen, K. (1991). The polarization lidar technique for cloud research: A review and

current assessment. *Bulletin of the American Meteorological Society*, *72*(12), 1848-1866. doi: 10.1175/1520-0477(1991)0722.0.co;2

Sassen, K., & Khvorostyanov, V. (1998). Radar probing of cirrus and contrails: Insights from 2d model simulations. *Geophysical Research Letters*, *25*(7), 975-978. doi: 10.1029/98gl00731

Sassen, K., Wang, Z., & Liu, D. (2008). Global distribution of cirrus clouds from cloudsat/cloud-aerosol lidar and infrared pathfinder satellite observations (calipso) measurements. *Journal of Geophysical Research*, *113*. doi: doi:10.1029/2008jd009972

Schuddeboom, A., McDonald, A. J., Morgenstern, O., Harvey, M., & Parsons, S. (2018). Regional regime-based evaluation of present-day general circulation model cloud simulations using self-organizing maps. *Journal of Geophysical Research: Atmospheres*, *123*(8), 4259-4272. doi: 10.1002/2017jd028196

Schuddeboom, A., Varma, V., McDonald, A. J., Morgenstern, O., Harvey, M., Parsons, S., ... Furtado, K. (2019). Cluster-based evaluation of model compensating errors: A case study of cloud radiative effect in the southern ocean. *Geophysical Research Letters*, *46*(6), 3446-3453. doi: 10.1029/2018gl081686

Scott, R., & Lubin, D. (2014). Mixed-phase cloud radiative properties over ross island, antarctica: The influence of various synoptic-scale atmospheric circulation regimes. *Journal of Geophysical Research: Atmospheres*, *119*(11), 6702-6723. doi: doi:10.1002/2013jd021132

Silber, I., Verlinde, J., Cadeddu, M., Flynn, C. J., Vogelmann, A. M., & Eloranta, E. W. (2019). Antarctic cloud macrophysical, thermodynamic phase, and atmospheric inversion coupling properties at mcmurdo station—part ii: Radiative impact during different synoptic regimes. *Journal of Geophysical Research: Atmospheres*, *124*(3), 1697-1719. doi: 10.1029/2018JD029471

Silber, I., Verlinde, J., Eloranta, E. W., & Cadeddu, M. (2018). Antarctic cloud macrophysical, thermodynamic phase, and atmospheric inversion coupling properties at mcmurdo station: I. principal data processing and climatology. *Journal of Geophysical Research: Atmospheres*, *123*(11), 6099-6121. doi: 10.1029/2018jd028279

Stephens, G., Vane, D., Boain, R., Mace, G., Sassen, ., K, Wang, Z., ... Mitrescu, C. (2002). The cloudsat mission and the a-train: A new dimension of space-based observations of clouds and precipitation. *Bulletin of the American Meteorological Society*, *83*(12), 1771-1790. doi: 10.1175/bams-83-12-1771

Stephens, G., Vane, D. G., Tanelli, S., Im, E., Durden, S., Rokey, M., ... Marchand, R. (2008). Cloudsat mission: Performance and early science after the first year of operation. *Journal of Geophysical Research: Atmospheres*, *113*. doi: 10.1029/2008jd009982

Tanelli, S., Durden, S. L., Im, E., Pak, K. S., Reinke, D. G., Partain, P., ... Marchand, R. T. (2008). Cloudsat's cloud profiling radar after two years in orbit: Performance, calibration, and processing. *IEEE Transactions on Geoscience and Remote Sensing*, *46*(11), 3560-3573. doi: 10.1109/tgrs.2008.2002030

Trenberth, K. E., & Fasullo, J. T. (2010). Simulation of present-day and twenty-first-century energy budgets of the southern oceans. *Journal of Climate*, *23*(2), 440-454. doi: 10.1175/2009jcli3152.1

Vergara-Temprado, J., Miltenberger, A., Furtado, K., Grosvenor, D., Shipway, B., Hill, A., ... Carslaw, K. (2018). Strong control of southern ocean cloud reflectivity by ice-nucleating particles. *Proceedings of the National Academy of Sciences*, *115*(11), 2687-2692. doi: 10.1073/pnas.1721627115

Wang, Z. (2019). *Cloudsat 2b-cldclass-lidar product process description and interface control document.* Retrieved from `http://www.cloudsat.cira.colostate.edu/sites/default/files/products/files/2B-CLDCLASS-LIDAR_PDICD.P1_R05.rev0_.pdf`

Widener, K., Bharadwaj, N., & Johnson, K. (2012). Ka-band arm zenith radar

(kazr) instrument handbook. *United States Department of Energy*. doi: doi:10.2172/1035855

Winker, D., Hunt, W. H., & McGill, M. J. (2007). Initial performance assessment of caliop. *Geophysical Research Letters*, *34*(19). doi: 10.1029/2007gl030135

Winker, D., Vaughan, M., Omar, A., Hu, Y., & Powell, K. (2009). Overview of the calipso mission and caliop data processing algorithms. *Journal of Atmospheric and Oceanic Technology*, *26*(11), 2310-2323. doi: 10.1175/2009jtecha1281.1

Zhang, D., Wang, Z., & Liu, D. (2010). A global view of midlevel liquid-layer topped stratiform cloud distribution and phase partition from calipso and cloudsat measurements. *Journal of Geophysical Research*, *115*. doi: 10.1029/2009jd012143

**Figure 1.**

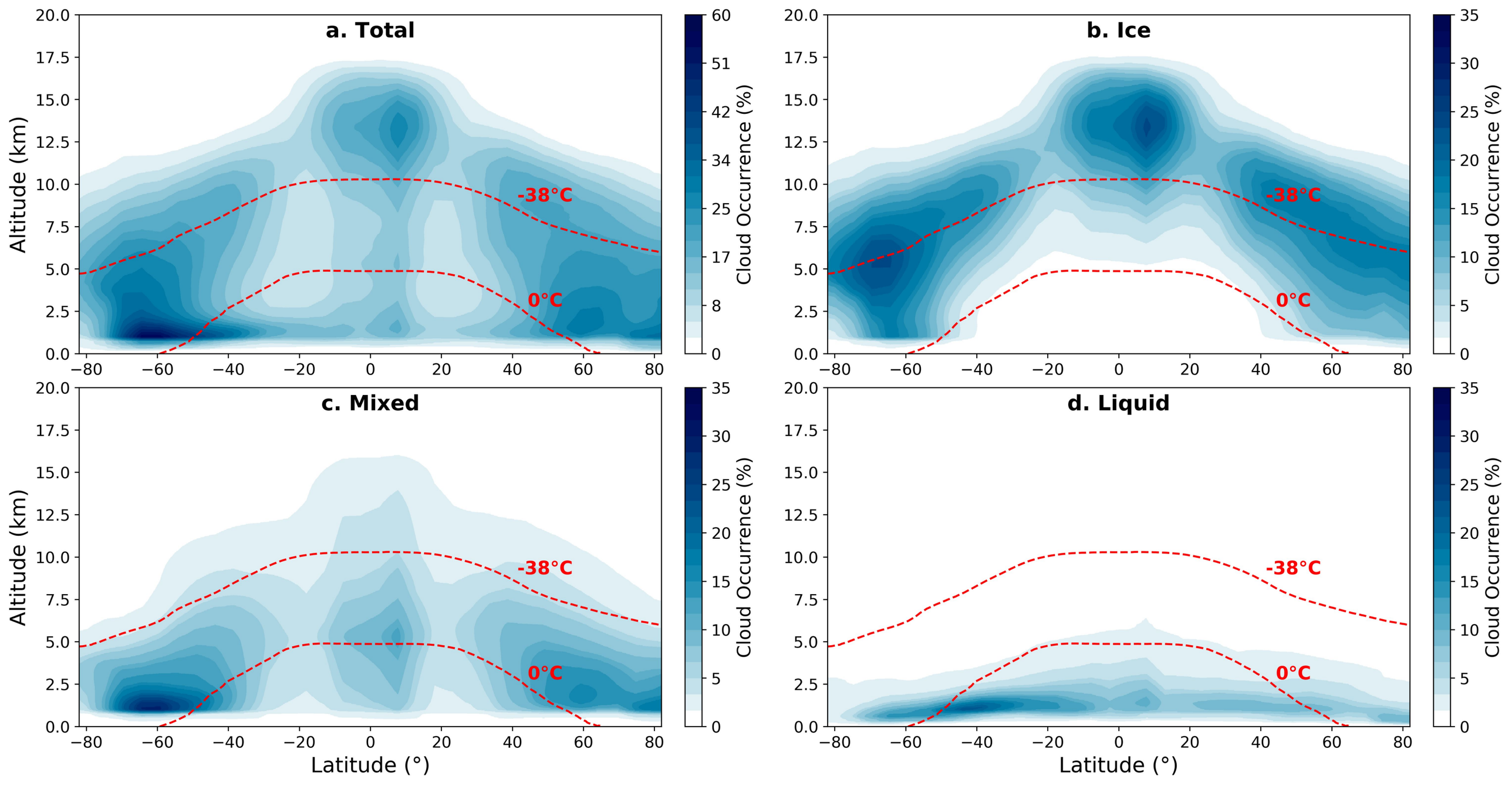
a. Total
b. Ice
c. Mixed
d. Liquid
-38°C
0°C
Altitude (km)
Latitude (°)
Cloud Occurrence (%)
20.0
17.5
15.0
12.5
10.0
7.5
5.0
2.5
0.0
−80
−60
−40
−20
0
20
40
60
80
60
51
42
34
25
17
8
0
35
30
25
20
15
10
5
0

**Figure 4.**

a. 2BCL5 $^{c}$ ∩ AWARE

b. DARDAR $^{c}$ ∩ AWARE

c. a - b

d. AWARE $^{c}$ ∩ 2BCL5

e. AWARE $^{c}$ ∩ DARDAR

f. d - e

g. AWARE ∩ 2BCL5

h. AWARE ∩ DARDAR

i. g - h

Altitude (km)

Detection Frequency (%)

Difference (%)

**Figure 7.**

AWARE Radiosonde

ECMWF-AUX

a.

b.

c.

d.

e.

f.

Ice
Mixed
Liquid
Unknown

2BCL5

DARDAR

AWARE

Normalised Cloud Occurrence (%)

Temperature (°C)

Temperature (°C)

**Figure 2.**

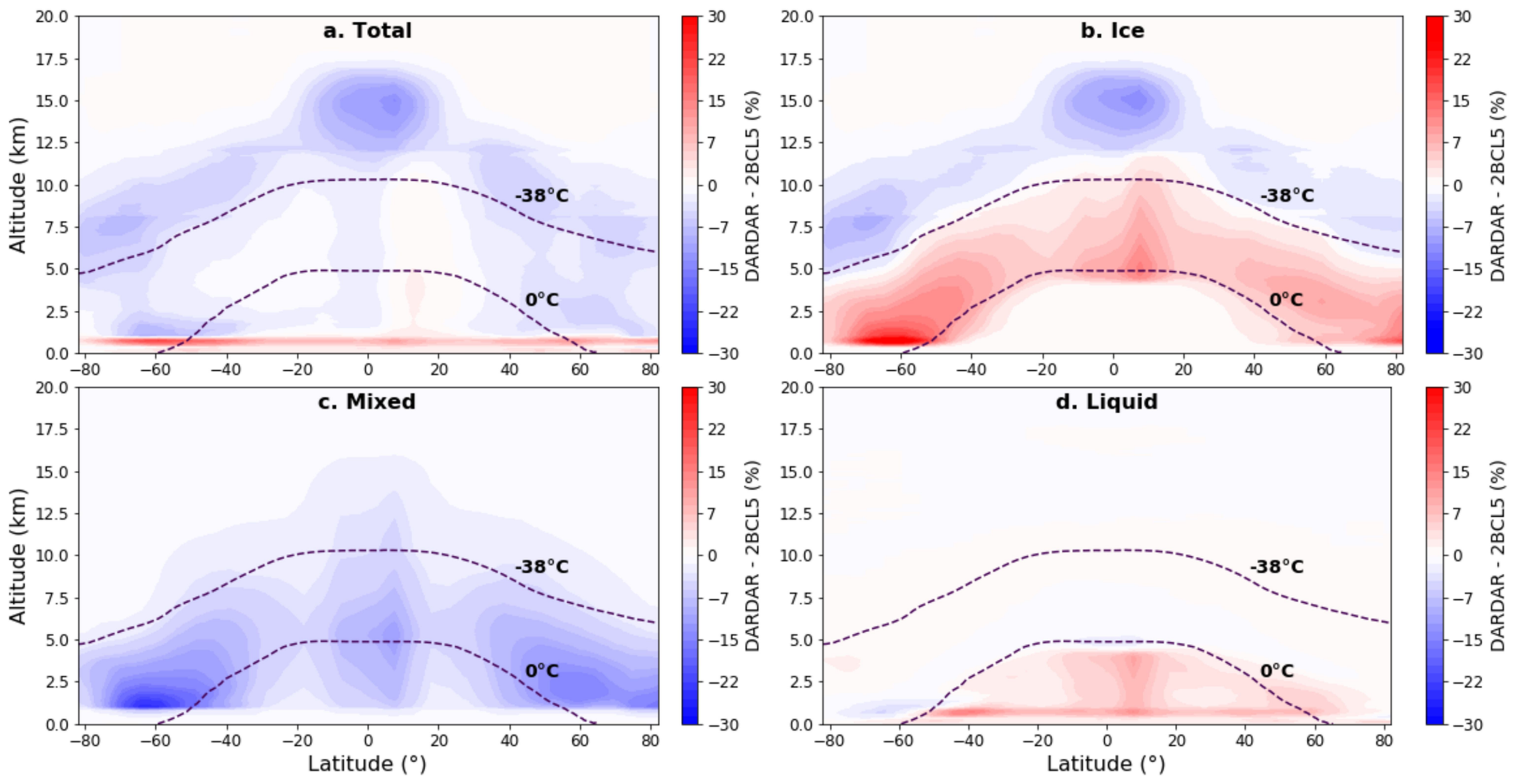
a. Total
b. Ice
c. Mixed
d. Liquid
-38°C
0°C
Altitude (km)
Latitude (°)
DARDAR - 2BCL5 (%)
20.0
17.5
15.0
12.5
10.0
7.5
5.0
2.5
0.0
−80
−60
−40
−20
0
20
40
60
80
30
22
15
7
0
−7
−15
−22
−30

**Figure 3.**

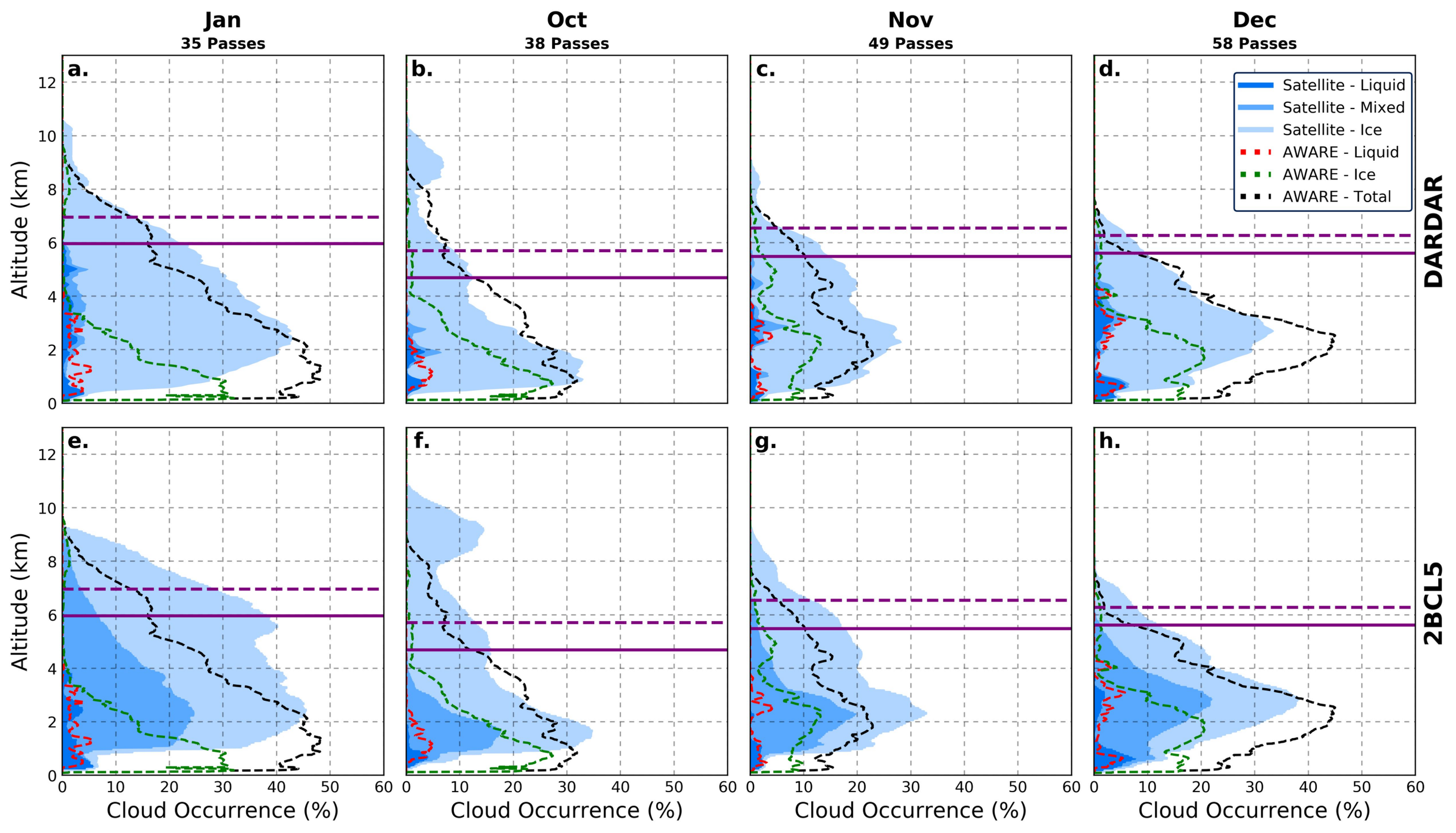
Jan
35 Passes
Oct
38 Passes
Nov
49 Passes
Dec
58 Passes
a.
b.
c.
d.
e.
f.
g.
h.
Satellite - Liquid
Satellite - Mixed
Satellite - Ice
AWARE - Liquid
AWARE - Ice
AWARE - Total
DARDAR
2BCL5
Altitude (km)
Cloud Occurrence (%)
0
2
4
6
8
10
12
0
10
20
30
40
50
60

**Figure 5.**

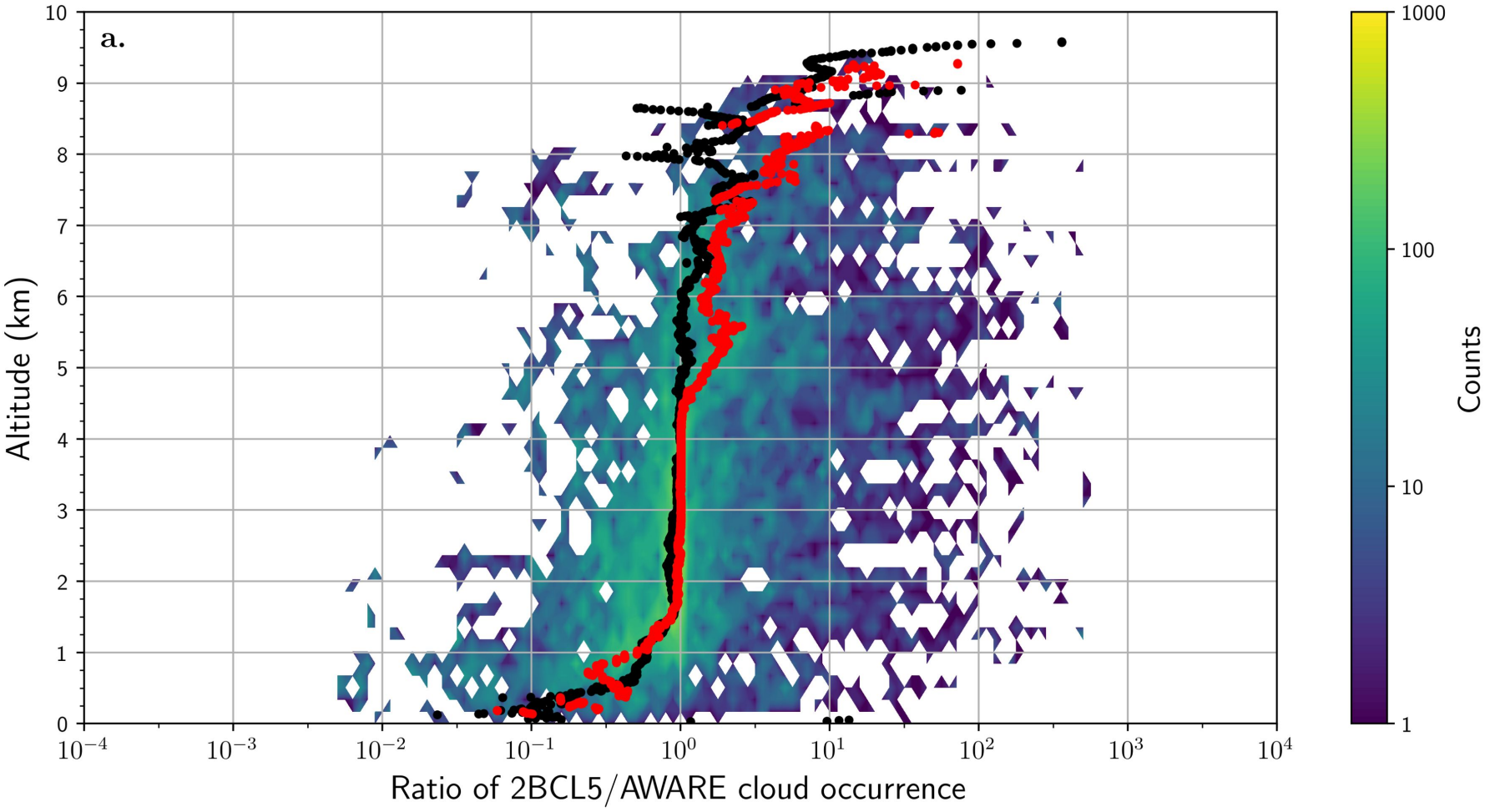
a.
Altitude (km)
Ratio of 2BCL5/AWARE cloud occurrence
Counts
b.
Altitude (km)
Ratio of DARDAR/AWARE cloud occurrence
Counts
c.
Altitude (km)
Ratio of 2BCL5/DARDAR cloud occurrence
Counts

**Figure 6.**

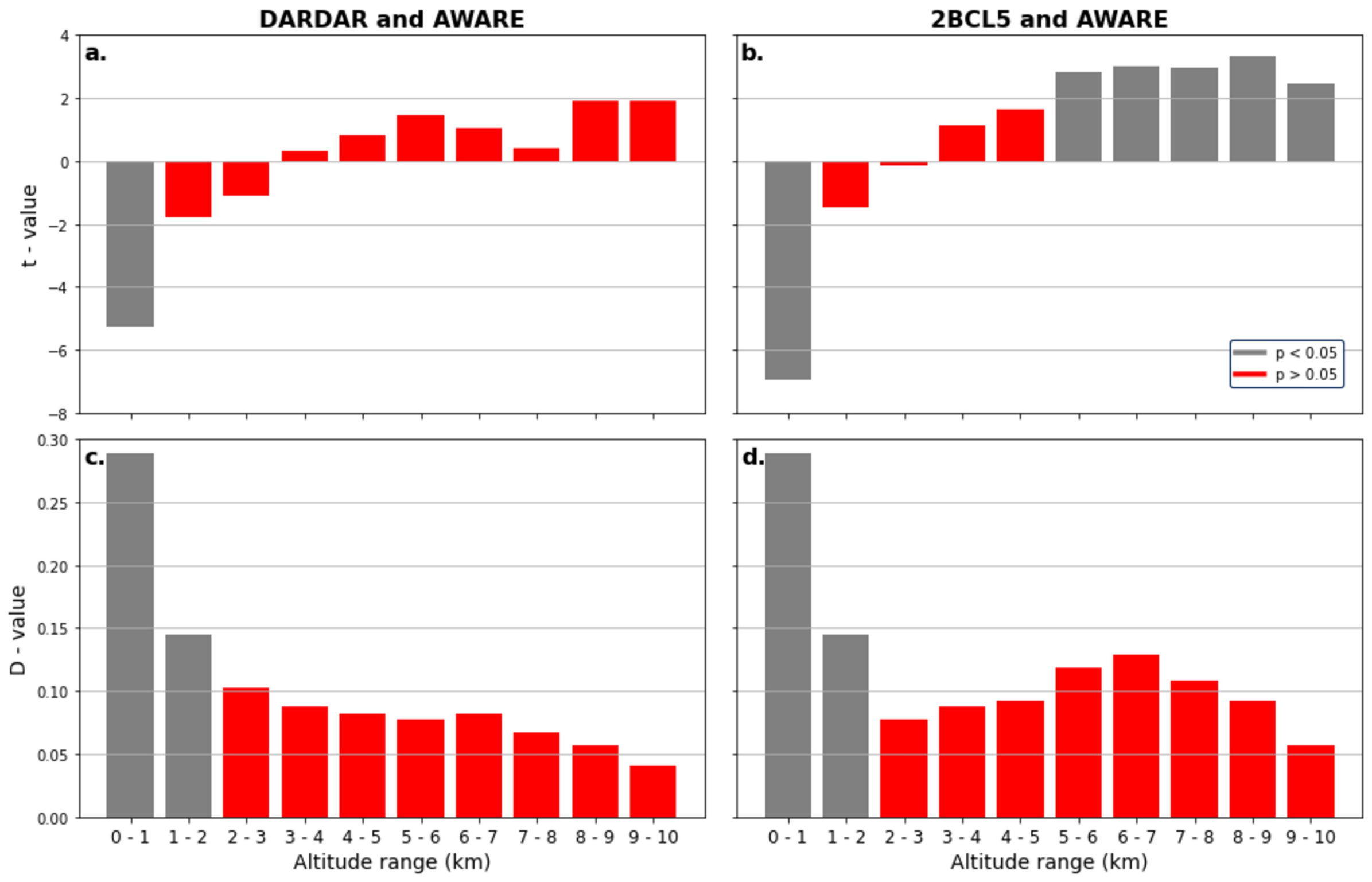
DARDAR and AWARE
2BCL5 and AWARE
a.
b.
c.
d.
t - value
D - value
p < 0.05
p > 0.05
4
2
0
−2
−4
−6
−8
0.30
0.25
0.20
0.15
0.10
0.05
0.00
0 - 1
1 - 2
2 - 3
3 - 4
4 - 5
5 - 6
6 - 7
7 - 8
8 - 9
9 - 10
Altitude range (km)
Altitude range (km)